

A Numerical and Experimental Comparative Study on the Performance of
Organic and Metallic Phase Change Materials under High Power
Millisecond Pulses

By

David González Niño

A thesis submitted in partial fulfillment of requirements for the degree of

Master of Science

in

Mechanical Engineering

at the

University of Puerto Rico
Mayagüez Campus

May 2017

Approved by:

Pedro O. Quintero, Ph.D.
President, Graduate Committee

Date

Paul Sundaram, Ph.D.
Member, Graduate Committee

Date

Ricky Valentín, Ph.D.
Member, Graduate Committee

Date

Pedro Vasquez Urbano, Ph.D.
Representative of Graduate Studies

Date

Paul Sundaram, Ph.D.
Chairman of the Department

Date

Abstract

Phase changes materials (PCMs) have been studied as passive cooling alternative for different conditions. Due to the US Army need for the development of a passive cooling system alternative for pulsed power applications, this research studies the performance of PCMs as passive cooling for pulsed power applications.

An unidimensional simple model, easy to implement and use, was developed. This model was used to guide and bring understanding on how different materials would perform under different conditions. This model studied the performance, under typical high power short pulse condition, of two organic PCMs (erythritol and n-octadecane), three metallic PCMs (gallium, Bi/Pb/Sn/In and indium) and a silicone dielectric gel. Finite difference method and heat integration method were used to model the heat transfer and melting process. The model showed that metallic PCMs would outperform another material, compared to organic PCMs and dielectric gel, under high power fast transient pulses. The model also shows that high thermal conductivity is beneficial for fast transient, however, this benefit will decrease if using a same energy pulse at longer time, where latent heat of fusion would dominate over thermal conductivity. Once it was known what expect, these results were verified via experimentation.

A device that work as heater and temperature sensor was developed to perform the experimental evaluation of metallic PCMs. During the experimentation, metallic PCM, as the model suggested, outperformed organic PCMs and dielectric gel under high power fast pulse condition. An outstanding temperature suppression 80°C was achieved by a metallic PCM (Fields'metal) compared to dielectric gel under a pulse of 160W

(338W/cm²). This study shows the great benefit of using metallic PCMs as passive cooling for pulsed power applications.

Resumen

Los materiales de cambio de fase (PCMs, por sus siglas en inglés) han sido sujeto de estudios como sistemas de enfriamiento pasivo, para diferentes tipos de aplicaciones. Debido a la alta demanda de soluciones pasivas para enfriamiento en aplicaciones de electrónica de pulsos, éste trabajo estudia el beneficio que podría tener la implementación de este tipo de materiales como sistema de enfriamiento para las aplicaciones antes mencionadas.

Un modelo numérico unidimensional fue desarrollado. Este modelo fue utilizado para brindar un mayor entendimiento en la posible ejecutoria que pudieran tener bajo diferentes condiciones. Con este modelo, se estudió el desempeño de dos materiales orgánicos (erythritol y n-octadecano), dos aleaciones de bajo punto de fusión (Bi/Pb/Sn/In y Bi/Sn/In) y un gel dieléctrico. La ecuación de calor se utilizó para modelar la transferencia de calor en el sistema y el método de integración de calor fue utilizada para modelar el cambio de fase (derretimiento). El modelo mostró que las aleaciones de bajo punto de fusión tendrían un mejor desempeño que el que tendría un PCM orgánico y el dieléctrico en pulsos de alta potencia y en la escala de milisegundos. También mostró que, si fijamos una energía para un pulso y variamos los tiempos de pulso, la conductividad termal dominaría el desempeño de un material en pulsos cortos, pero, a pulso más largos, el calor latente sería quien dominaría el desempeño del material. Una vez entendido lo que se podría esperar, se procedió a la verificación de los resultados por experimentación.

Un dispositivo capaz de funcionar como fuente de calor y medidor de temperatura fue diseñado y fabricado para evaluar el desempeño de los PCMs. Los resultados del

experimento confirmaron lo que el modelo había sugerido, que las aleaciones de bajo punto de fusión tuvieron un desempeño superior a los demás materiales. Una disminución de 80°C se puede observar cuando se compara la aleación Bi/Sn/In y el material dieléctrico, bajo un pulso de 160W (338W/cm²). Este estudio demuestra el gran beneficio de utilizar materiales de bajo punto de fusión como sistema de enfriamiento pasivo para aplicaciones de electrónica de pulso.

© David González Niño 2017

Dedictory

Para mi mamá, a quién le debo todo lo que soy.

... porque dió e hizo el todo por el todo para yo poder alcanzar lo que soy.

... porque me enseñó que no hay dificultades que no se pueden sobrepasar.

... porque ella es mi inspiración.

To my mom because I owe her everything that I am.

... because she gave and did everything so I can be who I am.

... because she taught me that there are no difficulties that we can't overpass.

... because she is my inspiration.

Acknowledgment

First, I would like to thank my advisor, Dr. Pedro O. Quintero Aguiló, who put a lot of trust in me from the very beginning, for his support, advice, and counsel. I will be always thankful for your patience and availability to talk every time that I needed to. THANKS!

To all my friends and family, who had been there for me every time that I needed them.

To my mentors at Army Research Laboratory, Dimeji Ibitayo, Dr. Lauren M. Boteler and Nick Jankowski, and all my coworkers at ARL.

-David González Niño

This work was funded by Maryland office of Oak Ridge Associated Universities (**ORAU**), Department of Energy's Oak Ridge Institute for Science and Education (**ORISE**), and the collaborative agreement UPRM-ARL Award W911NF-16-2-0063.

Contents

1. Justification	1
2. Literature Review	4
3. Objectives	10
4. Methodology.....	11
4.1 Numerical study	11
4.1.1 Equations.....	12
4.1.2 Validations.....	16
4.1.3 Results and Analysis	17
4.1.4 Conclusion	23
4.2 Heater/RTD.....	24
4.2.1 Design	25
4.2.2 Fabrication.....	28
4.2.3 Packaging.....	28
4.2.4 Calibration	30
4.2.5 Test	32
4.2.6 Conclusion	33
4.3 High Power Pulse experiment	34
4.3.1 Experiment procedure.....	35
4.3.2 Results and discussion.....	36
4.3.3 Conclusion	43
5. Conclusion.....	45
6. Reference.....	47
Appendix A	51
Appendix B	52
Appendix C	53
Appendix D	54
Appendix E	55
Appendix F.....	56

List of Figures

Figure 1: Visual representation of model	12
Figure 2: Sequence of the equation used during the melting process.	16
Figure 3: Comparison between the model and the experimental data from Zivkovic and Fuji [32]	17
Figure 4: Result using the pulse condition #1.	19
Figure 5: Temperature comparison using pulse condition #2.....	20
Figure 6: Performance of different materials under the pulse condition #3.....	21
Figure 7: Comparison of using a metallic PCM (Bi/Pb/Sn/In) and an organic PCM (erythritol) at same energy pulse but different length.....	22
Figure 8: A visual illustration of the challenge of using a thermocouple on a flat surface.	24
Figure 9: Illustration of the final design. In blue (thin lines) is shown the RTD and in red (thick lines) the heater.	27
Figure 10: A sample of a fabricated device.	28
Figure 11: Digital representation of the final device with the plastic PCM container.....	29
Figure 12: Sequence of the package preparation.	29
Figure 13: Temperature - resistance calibration curve of three different devices.....	31
Figure 14: Result of two devices pulsed with a 31W and near to 20 ms pulse without any PCM or encapsulant on top.	32
Figure 15: Process diagram on how the experiment is done.....	36
Figure 17: Performance of different materials subjected to a high power short pulses. A) Result from a pulse of 120 W. B) Results from a pulse of 160 W C) Results from a pulse of 280 W..	40
Figure 18: Thermal benefit of using Bi/Pb/Sn/In over PureTemp 58x.	42
Figure 19: Power input thru time of Bi/Pb/Sn/In and dielectric gel.....	43

List of Tables

Table 1: List of the studied materials and their properties.....	18
Table 2: List of the studied conditions.	18
Table 3: Final dimensions for the heater/RTD device.	27
Table 4: Numerical calibration data of three devices.	31
Table 5: List of material used during experiment and their properties.	34
Table 6: Numerical data from Figure 16.....	38
Table 7: Numerical data from Figure 17.....	41

NOMENCLATURE

k	Thermal conductivity	$W/(m \cdot K)$
A	Area	m^2
Δx	node thickness	m
ρ	Density	kg/m^3
c_p	Specific heat	$kJ/(kg \cdot K)$
T_m	Melting temperature	$^{\circ}C$
Fo	Fourier number	
V	Volume	m^3
α	Thermal diffusivity	m^2/s
Δt	Time step	s
T	Temperature	$^{\circ}C$
f_l	Liquid fraction	
H	Convection coefficient	$W/(m^2 \cdot K)$
H	Latent heat of fusion	kJ/kg
q	Heat flux	W/m^2
T_{∞}	Ambient temperature	$^{\circ}C$
TCR	Temperature Coefficient of Resistance	$1/^{\circ}C$
PCM	Phase Change Material	
RTD	Resistance Temperature Detector	
<i>Subscripts:</i>		
n	Node number	
s	Solid	
l	Liquid	
mp	Melting process	

1. JUSTIFICATION

In 1965, Gordon E. Moore published an article where he predicted what will be, more or less, the trend onto integrated circuits, the number of components in an integrated circuit will double every year [1]. In terms of electronics, this means that every year electronics will shrink in size, but not in power, a combination that makes thermal management even more challenging and, not only because there will be a smaller surface area available to remove heat, but also because even more heat will be needed to be removed. Electronic thermal management has been very well studied throughout the years but still, 55% of power electronic failures are catalogued as temperature related failures [2].

The most common way to address electronic thermal management is reducing the thermal resistance. A reduction in thermal resistance results in a reduction in average device temperature. In applications where size is a limitation, is common to reduce material in order to decrease the thermal resistance. However, by reducing on material, the thermal inertia, which is the responsible of preventing rapid change in temperature [3-4], will also be reduced. However, in some power electronics, which are subjected to milliseconds high power pulses, the reduction of thermal inertia can be harmful [4, 5]. Traditionally for pulsed power applications, the cooling system is overdesigned in order to manage temperature peaks [5,6], resulting in an increment of size, weight and power (SWaP) requirement. The integration of phase change materials (PCMs) as possible thermal solution for pulsed power applications has been widely studied.

Phase change materials are any material that undergoes a phase transformation, melting in this case, within the temperature range of application. Melting is an isothermal process, where the energy is absorbed by latent heat and there is little to none increment on temperature. During 1971 a report was developed for NASA in the use of PCM for thermal control in space vehicles [7]. Organic PCMs are one of the most common PCM used; their known thermos-physical properties, low cost, high latent heat of fusion by mass, and availability in a wide range of temperature [7], make them preferable and suitable for a lot of applications. However, the inherent low thermal conductivity in organic PCMs is commonly mentioned as a great disadvantage on these materials [8]. Thermal enhancers such as heat sinks [9], metal meshes and foams [10-11], graphite nanofibers [12] and metal honeycombs [13-14] have been widely used and studied to improve, with limited result, the thermal conductivity of these systems. The use of metallic PCMs, which naturally have high thermal conductivity can even perform better than an organic PCM embedded in a metal foam [15].

High density in metallic PCMs and the complexity of integrating metallic PCMs, are mentioned as a downside of this type of PCMs. However, recent studies have highlight the use of metallic PCMs in application where thermal response is of a paramount of importance and the mass is not a big concern, such as compact and high heat rate application [16,17].

This project aims to study the performance of metallic PCMs under fast high heat milliseconds pulse applications. The study includes a numerical based designing tool able to estimate the performance of different PCMs under different pulse conditions (PCM thickness, power and pulse width). The numerical evaluation was used to guide the

material selection for the experimental study. A device capable of working as a heater and as temperature monitor was designed and fabricated, using the Army Research Laboratory clean room facilities. This device mimics a chip subjected to high power transient pulses for the experimental study. At last, an experimental study is included, guided by the numerical work and using the designed device. The experimental study aims to validate the results obtained by the numerical study.

2. LITERATURE REVIEW

PCMs have been studied for a wide area of applications as solar cooking [18], solar heater [19], building cooling [20-21], to mention few. The ability of storing energy in latent heat form in order to release the energy later, smoothing peak loads and shifting peak loads, make PCMs good prospects for a wide range of thermal challenges. In the same way that PCMs had demonstrated a capacity to smooth or shift peak loads in building, PCMs have been studied as a passive cooling alternative for electronics applications.

Setoh et al. [9], used n-eicosane as a passive cooling system for mobile phone. In this study, four different heat sinks arrangements with different numbers of fins were used in order to study the effect of the number of fins on the performance of the PCM. First, PCM was subjected to a constant power of 3W, 4W and 5W for 120 minutes to studye to compare the performance of a heat sink with and without PCM. The heat sink that contained the PCM was able to maintain a lower temperature than the one without PCM. Then, the heat sinks were tested under different transient conditions in order to simulate a typical power consumption by a mobile phone. The study showed that, when compared to the arrangement without PCM, n-eicosane was able to maintain a lower maximum temperature. These results were achieved because the PCM undergoes by a phase transformation, absorbing energy as latent heat and decreasing the temperature increment throughout the melting period. The lower discharging rate in PCM heat sink arrangement was expected due to the energy release during the material's solidification. In this process, energy is released as the PCM is solidifying. Similar experiments have

been done under different power levels and using different solutions to enhance thermal conductivity in organic PCM.

The inherent low thermal conductivity on organic PCMs is the most common and recurrent concern, which makes the search for the most effective thermal enhancement in organic PCM as the most common research topic. In [12], graphite nanofibers were used in order to modify the thermal response of a paraffin wax. For this experiment, a large PCM container was intended to be used with the premise that “more PCM” means that “more energy can be absorbed for a high power application”. However, as the author mentions in the study, the low thermal conductivity in the PCM can lead to the isolation of the melt process near the heat source, making the PCMs located further from the heat source unusable. The use of graphite nanofiber, as thermal enhancer, improve the performance of the PCM module, heating in a more homogenous way thru all the PCM; ensuring the use of all PCM and eliminating the insulation barrier that can be developed by the low thermal conductivity. A metal (copper) foam was used in [11] as thermal enhancer for the paraffin wax RT58, resulting in a temperature hold for longer time compared to the same PCM without metal foam. The metal foam embedded with PCM not only was able to hold the temperature for longer time, but also was able to solidify in shorter time, which is crucial for transient applications, where PCM is needed in solid state prior to following pulses in order to melt and store energy by latent heat. Otherwise, if following pulses are made with liquid PCM, there is a high probability that the implementation of any PCM would be counterproductive. Could metallic PCMs, due to their naturally high thermal conductivity, perform better than organic PCMs?

Garimella, in [8], performed a study where the performance of a copper heat sink was compared to metal foam embedded with organic PCM (triacontane) and two metal PCMs (Bi/Sn/In and Bi/Pb/Sn/In). The metallic PCMs, by themselves, had a better performance holding a lower temperature for longer time when compared to the copper heat sink and triacontane with thermal enhancer. Although metallic PCMs showed a better performance than the other three options, the author raises the high density as a concern for considering metallic PCM as a passive cooling system. However, recent studies have pointed out that the high thermal conductivity on metallic PCMs balanced out the disadvantage related on weight penalty due to high mass density on applications where weight is not necessarily a critical concern [16,17].

Shamberger [22] defined a figure of merit (FOM) for the cooling capacity of PCMs. Organic PCMs and salt-hydrates have similar FOM, but in the other hand, metallic PCMs have a FOM an orders magnitude higher than non-metallic PCMs. This difference is driven by the difference in thermal conductivity on metallic PCM that could be one or two orders magnitude higher than non-metallic PCMs. Later, the author concluded that $k^{1/2}$ represent 92.8% of the variance of the FOM. Guided by this same FOM, Shao et al. [23] performed a study where a metallic PCM (49Bi/18Pb/12Sn/21In) and an organic PCM (paraffin wax) were inserted in a chip and they were compared to a chip without PCM. The FOM 2603 ($\times 10^3 \text{ W*s}/(\text{K*m}^4)$) was calculated for the metallic PCM and 22 ($\times 10^3 \text{ W*s}/(\text{K*m}^4)$) for the paraffin wax. They were pulsed with a pulse of 11W for 0.6 s. The metallic PCM was able to maintain a lower temperature, 14°C lower than the chip without PCM, showing a temperature suppression when it reached the melting temperature. In the other hand, the organic PCM did not show any thermal suppression, but it performed

even worse than the chip without any PCM. Therefore, the implementation of organic PCM was counterproductive in this application. Compact applications, such as mobile devices, are constrained by volume therefore the application of metallic PCMs have been considered as a possible solution for thermal management.

Ge and Liu in [24] studied the performance of different PCMs, n-eicosane, paraffin, a salt hydrate and gallium, on keeping cool a smartphone. For this experiment, a heater was used to simulate the heat produced by a smartphone and a case filled with PCM was used as the passive cooling system. Gallium, which is a low melting metal, was able to hold the temperature below the specified limit for longer time compared to the other PCMs. Previously, these same authors performed a similar experiment, but using a USB flash memory [25] as the cooling target. For this study, temperature development was measured, and the performances of the USB with gallium and without gallium were compared. The gallium-filled-USB showed a temperature lower than 29°C for 18 min, compared to the USB without gallium that reached temperature above 40°C in the same period of time. Other experiment with a compact application was conducted by Shao et. al. in [26], where Bi/In/Pb/Sn alloy was used as PCM. In this study, the performance of the metallic PCM was related to its ability to maintain a smartphone at a lower temperature during temporary power boosts. Bi/In/Pb/Sn alloy was compared to the same system without PCM, and it was demonstrated the productive ability of metallic PCM to, not only reduce temperature swings in the devices, but also maintain a lower temperature with a longer computational sprinting or power boost, when it was compared to the device without PCM. We can take the most of metallic PCM, taking advantage of their inherent

high thermal conductivity, however, the PCM integration method, could affect the thermal response of the PCM.

Up to this date, there is not a study known by the author that studies the effect on different PCM integration method on the thermal response or performance. However, it is known that any layer or distance between the heat source and the thermal solution, could be harmful to the performance of the cooling system. Any layer, between the heat source and cooling system, will represent a thermal resistance and a delay on the thermal response. Integration methods proposed by Ai-Gang et al. [27] and Li-Wu Fan [28] which consist in an aluminum square tube and an aluminum rectangle, respectively, filled with metallic PCM, could be beneficial in the simplicity and the amount of PCM that they could fit in. However, methods alike, may tend to be bulky, which can be an issue where volume can be a constraint and, also, a thermal resistance between the heat source and the PCM, the aluminum wall in these cases, may diminish the real performance of the PCM.

Soupremanien [6] proposed to integrate metallic PCMs in a direct bonding copper (DBC) level. This idea represents a major reduction in the thermal resistance between PCM and heat source. A possible issue with this method is the stress that the change in volume because the change in phase of the PCM, solid to liquid, or thermal expansion by the metallic PCM could exert on the ceramic. One of the main advantage of this method is the small distance between the heat source and PCM, but also, DBC are traditionally made of high thermal conductivity ceramic. In this study, the authors use alumina, but they could use aluminum nitride.

A more even aggressive integration method was proposed by Desai et al.[29] and Shao et al. [23, 26]. This method consists in performing a cavity inside of the device. This

method would eliminate any thermal resistance and any layer between the heat source and PCM. Theoretically, this method would take the most of the metallic PCMs, because there is not barrier that may delay the thermal response of the PCM. However, this method can be really challenging. Desai et al. number some of the challenges that they faced, most of them related to a wetting issue between the metallic PCM and the silicon substrate. This integration method would face a device design method, which can increase the complexity not only on the design but also in the fabrication, which could lead to a significant increase of cost.

This project aims to study the performance of metallic PCMs, under pulse of 40W-160W at 20 milliseconds, integrating the PCMs directly on top of the heat source. For this method, a small plastic container was printed, via additive manufacturing, and a thin layer of silicon nitride was deposited on the device. This method is similar to the one proposed by Desai et al. and Shao et al. but without the complexity of performing a cavity inside of the device.

3. OBJECTIVES

As a main goal, this research aims to develop a comparative study between the performance of metallic and organic PCMs under high power short pulses. In order to achieve that main goal, three other goals were needed: (1) the development of a numerical based designing tool, where the performance of any PCM can be virtually studied under any condition, (2) the development of a device capable of working as heat source and temperature sensor and (3) the evaluation, via experimentation, of different PCMs under high power short pulse.

4. METHODOLOGY

This study developed and used a 1-D heat transfer analysis to understand and guide the experiments. This numerical evaluation rise light on how materials would perform based on their properties. The advantage of the numerical evaluation is that it let us to explore different scenarios, fast and with low cost. Once we had a better understanding on what to expect, we moved into the development and fabrication of a device that can work as a heater and temperature sensor. These devices were calibrated and subjected to testing to prove their quality. Once they were tested, these devices were used to perform the experiments. Two metallic PCMs (Bi/Pb/Sn/In and Fields' metal), two organic PCMs (PureTemp29 and PureTemp58) and a dielectric gel were used for this study.

4.1 NUMERICAL STUDY

Numerical evaluations allow us to understand the performance of PCM under different conditions in an easy and quick way. A 1-D model was developed in order to understand how the thermo-physical properties of the material can affect the performance. By changing properties or pulse conditions, this tool provide a lot of invaluable information on how any PCM may perform on any condition. For this model, PCM is assumed to be directly on contact on the top of the heat source. The heat source is assumed as an aluminum nitride chip resistor that is subjected to convection at the backside. The top side of the PCM is subjected to natural convection. Heat integration method or post-iterative method [30] was used to model the phase change and the finite difference method [31] was used to model the heat transfer between the chip and the PCM.

4.1.1 EQUATIONS

A visual representation of the system modeled is shown in **Figure 1**. The system is divided in three types of nodes: exterior, interior, and heat source node.

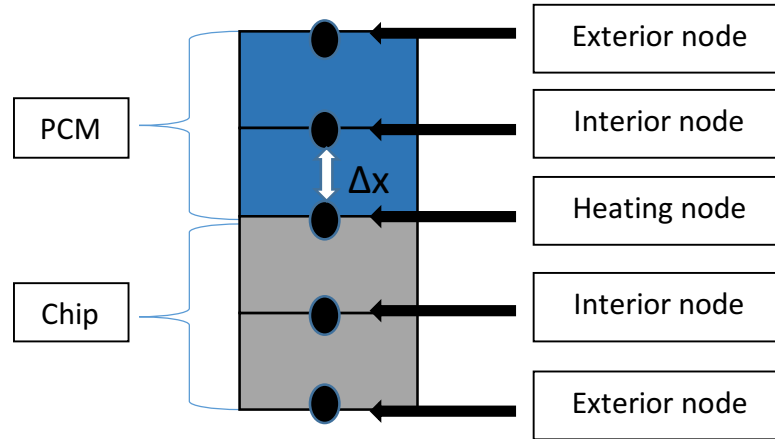


Figure 1: Visual representation of model

The exterior nodes (refers to **Figure 1**), which are located at the end of the system, are subjected to conduction heat transfer by the interior nodes and by natural convection. The exterior nodes are modeled using the Equation 1, that can be simplify using the Equation 2, where $Fo = \frac{\alpha \Delta t}{(\Delta x)^2}$ is the Fourier number, $\alpha = \frac{k}{\rho c_p}$ is the material thermal diffusivity and $Bi = \frac{h \Delta x}{k}$ is the Biot number [31].

$$hA(T_{\infty} - T_n^p) + \frac{kA}{\Delta x}(T_{n-1}^p - T_n^p) = \frac{\rho A c_p \Delta x}{2} \frac{(T_n^{p+1} - T_n^p)}{\Delta t} \quad (1)$$

$$T_n^{p+1} = 2Fo(T_{n-1}^p + BiT_{\infty}) + (1 - 2Fo - 2BiFo)T_n^p \quad (2)$$

The interior nodes, which are located between the heat source node and the exterior nodes, are subjected to conduction heat transfer and are modeled by the Equation 3, which can be simplified into Equation 4.

$$\frac{kA}{\Delta x}(T_{n-1}^p - T_n^p) + \frac{kA}{\Delta x}(T_{n+1}^p - T_n^p) = \rho A c_p \Delta x \frac{(T_n^{p+1} - T_n^p)}{\Delta t} \quad (3)$$

$$T_n^{p+1} = Fo(T_{n-1}^p + T_{n+1}^p) + (1 - 2Fo)T_n^p \quad (4)$$

The heat source node, which is located in the center of the system, is subjected to conduction heat transfer by the interior node of both sides and the heat generation of the system; this node is modeled using the Equation 5.

$$\frac{kA}{\Delta x}(T_{n-1}^p - T_n^p) + \frac{kA}{\Delta x}(T_{n+1}^p - T_n^p) = \left[\left(\frac{\rho A c_p \Delta x}{2} \right)_{chip} + \left(\frac{\rho A c_p \Delta x}{2} \right)_{PCM} \right] \frac{(T_n^{p+1} - T_n^p)}{\Delta t} \quad (5)$$

The heat source, unlike any other node where the thermo-physical properties only correspond to the PCM or chip, thermo-physical properties of both volume, chip and PCM, are used. Doing this, we try to place the heat generation between the PCM and chip, letting the thermo-physical properties of each material to distribute the energy through the system.

It is important to mention that this is an explicit method, the temperature is calculated based on the previous temperature, and a numerical stability is needed to keep

in consideration [31]. In order to comply with a numerical stability, Equation 6 must be satisfied every time for both materials, chip and PCM.

$$Fo(1 + Bi) \leq 0.5 \quad (6)$$

In order to model the phase transformation, the heat integration method or post-iterative method, described on [30] was used, which is presented in Equation 7.

$$\Delta T C_p = H \quad (7)$$

For this method, the temperature of every node was monitored. When one of the node pass the melting temperature, it is considered that the node enters to the melting transformation. Once the node entered the melting transformation, any temperature above the melting temperature is accounted as the latent heat absorbed by the phase change, as described in Equation 8, where Equation 9 described the percent of liquid present in the node and Equation 10 is the total latent heat of fusion in the node.

$$H_{ts} = (1 - f_l)\rho_s V c_{p,s} \Delta T + f_l \rho_l V c_{p,l} \Delta T \quad (8)$$

$$f_l = \frac{\sum H_{ts}}{H_{total}} \quad (9)$$

$$H_{total} = \rho_s \cdot A \cdot \Delta x \cdot H \quad (10)$$

After the amount of energy is accounted as latent heat, the temperature of the node is set back to the melting temperature in order to model the isothermal process of

phase change. The node temperature is hold at melting temperature until the amount of energy accounted as latent heat, is equal to the latent heat in that node's volume ($f_l = 1$) which means that the node is complete on liquid phase.

During the phase change, the amount of liquid in the node is monitored in order to change as well the physical properties – Equation 11-, taking in consideration the percent of liquid present at each iteration (Equation 9). To change the properties during the melting period, a Fourier number is calculated within each iteration, changing the thermal diffusivity. Equation 12 describe how thermal diffusivity is changed with every iteration. The melting node is assumed to start completely solid ($f_l = 0$), but as is considered that the previous node is in liquid, and the next node is completely solid, it is assumed that the thermal diffusivity will be composed as 25% material's liquid thermal diffusivity (from previous node), 25% material's solid thermal diffusivity (next node) and 50% of material's thermal diffusivity that will be changing by the amount of liquid in the node, as stated in Equation 12. An illustration on how this method is applied is shown at the **Figure 2**.

$$Fo_{mp} = \frac{\alpha_{mp}\Delta t}{(\Delta x)^2} \quad (11)$$

$$\alpha_{mp} = .25\alpha_l + .25\alpha_s + .5(f_l\alpha_l + (1 - f_l)\alpha_s) \quad (12)$$

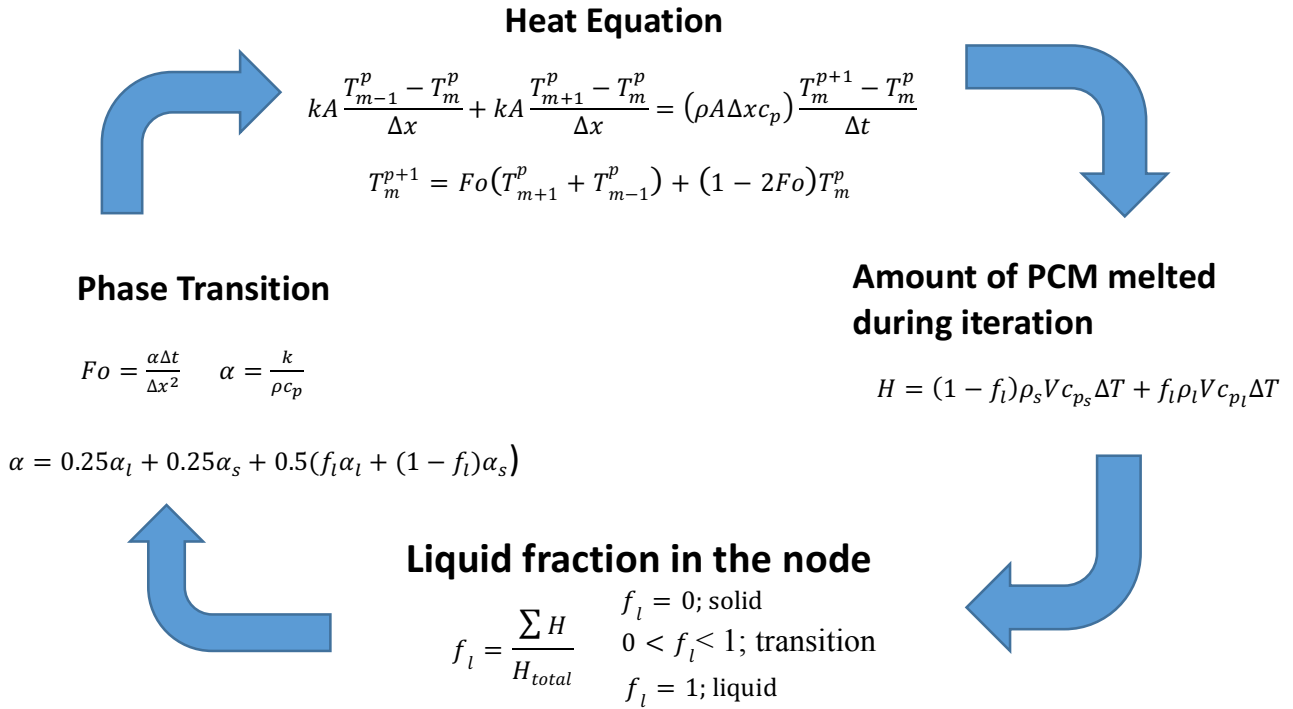


Figure 2: Sequence of the equation used during the melting process.

4.1.2 VALIDATIONS

Experimental data from Zivkovic and Fuji [32] was used to compare with the model. As shown in **Figure 3**, the model shows good agreement with the experimental data. A better agreement can be achieved by increasing the number of nodes.

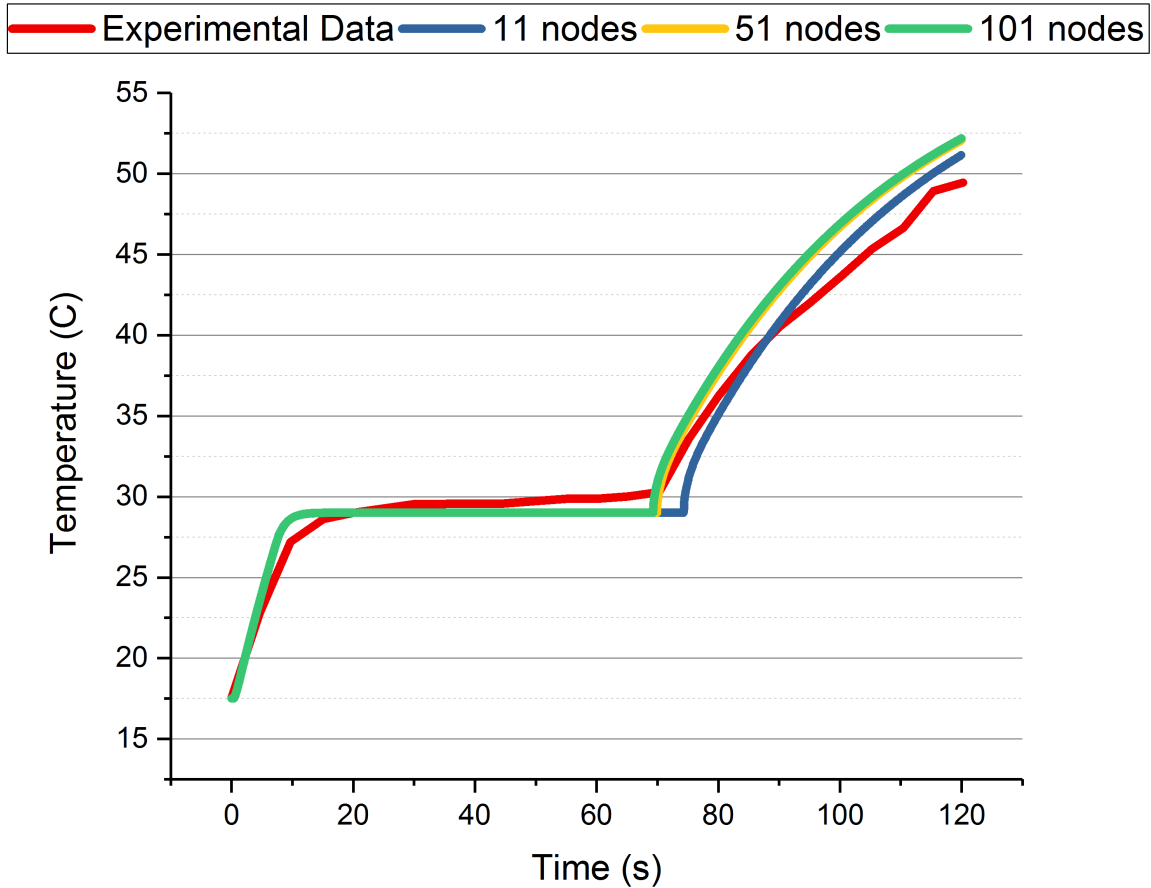


Figure 3: Comparison between the model and the experimental data from Zivkovic and Fuji [32]

4.1.3 RESULTS AND ANALYSIS

The scope for this model is to be able to make a quick study on the performance of different PCM, that are directly in contact with the heat source, a chip in this case, and compare them using a silicone dielectric gel as baseline. It was assumed a heat source with an area of 1 cm x 1 cm and 1.25 mm thick. Aluminum nitride is the material selected as the chip's substrate. A thickness of 0.1016mm thickness was assumed for the PCM and dielectric gel. **Table 1** list the material used during the study and their properties while **Table 2** shows the conditions used to make the study.

Table 1: List of the studied materials and their properties.

Material	T_m (°C)	k_s W/(m·K)	k_l W/(m·K)	ρ_s kg/m ³	ρ_l kg/m ³	$C_{p,s}$ kJ/(kg·K)	$C_{p,l}$ kJ/(kg·K)	H MJ/m ³	Ref
Aluminum Nitride		170		3260		0.740			
Encapsulant		0.576		1185		1465			[33]
PCMs									
Erythritol	117	0.733	0.326	1480	1300	1.383	2.765	466	[16]
n-octadecane	27.5	0.15	0.15	814	774	1.900	2.300	198	
Gallium	29.8	33.7	29.4	5903	6093	0.340	0.370	473	
Bi/Pb/Sn/In	57.0	33.2	10.6	9060	8220	0.323	0.721	267	

Table 2: List of the studied conditions.

#	T_∞ (°C)	Power (kW)	\dot{q} (MW/m ²)	h_{chip} (W/(m ² ·K))	h_{PCM} (W/(m ² ·K))	Time (s)
1	25	1.633	16.33	100	10	0.020
2	35	1.633	16.33	100	10	0.020
3	25	3.333	33.33	100	10	0.001

Figure 4 shows the result using the pulse condition #1 (refers to **Table 2**). During this condition, metallic PCMs outperform organic PCMs and dielectric gel. Bi/Pb/Sn/In have the lowest maximum temperature with 145°C, which represent a 12% improvement compared to the dielectric gel. Organic PCM, n-octadecane, which has the lowest melting temperature, ended with the worst performance. Erythritol, which has almost twice the latent heat of fusion, compared to Bi/Pb/Sn/In, did not perform as well as the metallic PCM. This suggest that the high thermal conductivity on metallic PCM could be the property to take in consideration for high power short pulses. However, possessing the high thermal conductivity or latent heat of fusion, as in case of gallium, does not guarantee the best performance. Gallium, having a very low melting temperature, started melting

from the very beginning of the pulse, which resulted in a complete melt of the PCM and therefore did not perform better than Bi/Pb/Sn/In.

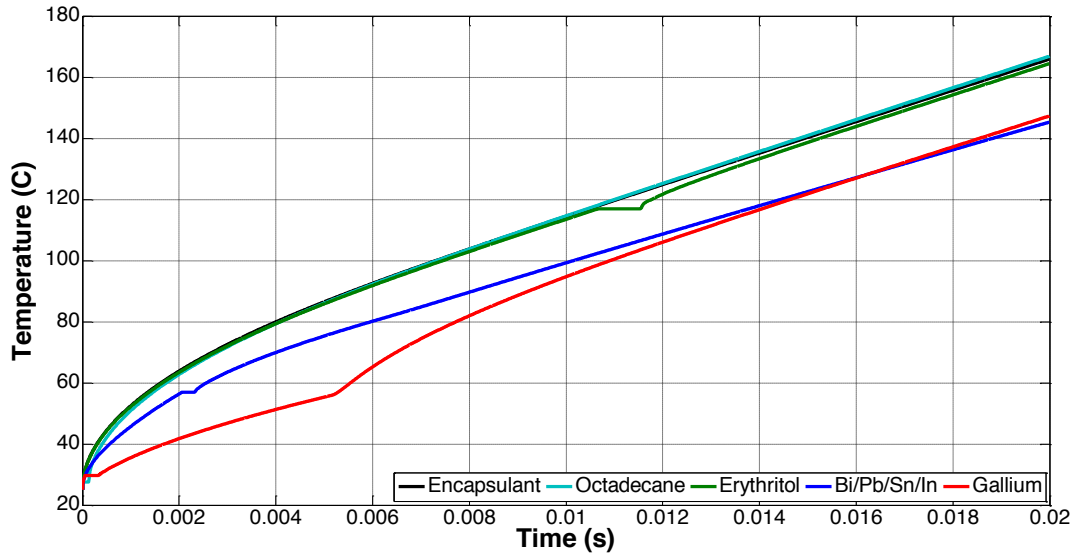


Figure 4: Result using the pulse condition #1.

Knowing how the performance could be temperature of application dependent, the condition #1 was done, but assuming 35°C as the ambient temperature. Under this condition, gallium and n-octadecane are at liquid state, therefore there is no phase transformation. **Figure 5** shows the performance under the pulse condition #2. Comparing the result from **Figure 5** and **Figure 4** it is clear how choosing a PCM that is not suitable for the temperature of application, can affect negatively its performance. Gallium being one of the best performer from the previous conditions, now performed similar to erythritol. This demonstrate that the material selection has to take in consideration, not only the thermo-physical properties, but also the temperature of application.

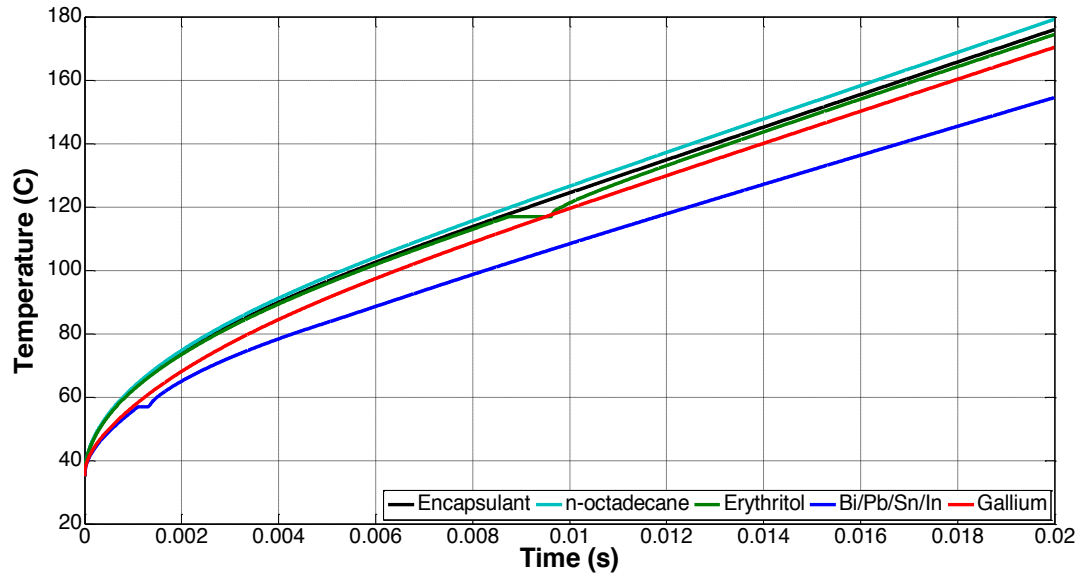


Figure 5: Temperature comparison using pulse condition #2.

Figure 6 shows the performance of different PCM under a 1 ms pulse of 3.33kW of power. Under this condition, metallic PCM were more suitable than any other material. In this case, compared to the one on **Figure 4**, the low melting temperature on gallium became the key on the performance of this material. The incorporation of gallium under this condition could lead to an improvement of 37.5% compared to dielectric gel.

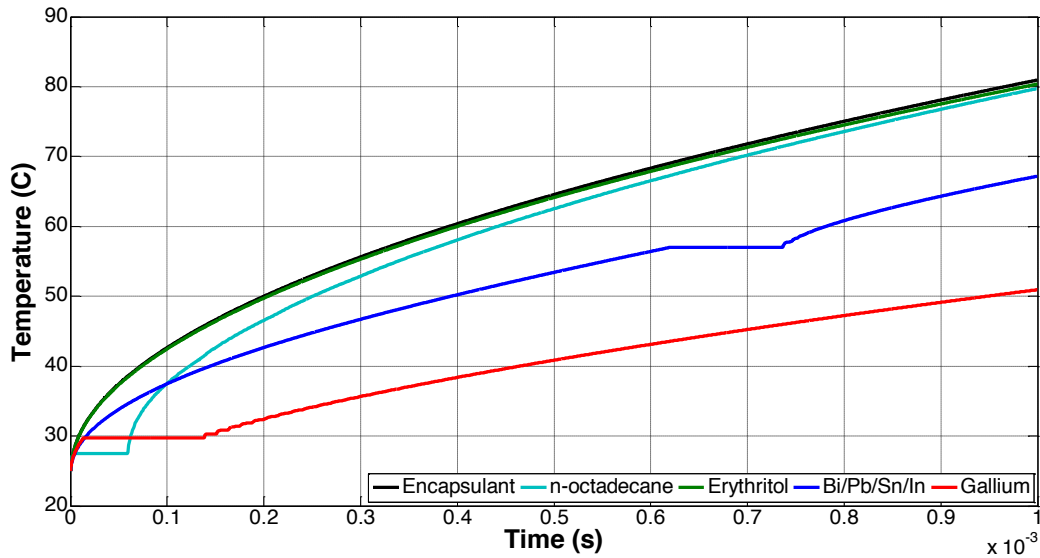


Figure 6: Performance of different materials under the pulse condition #3.

Up to this point, it is demonstrated that metallic PCM outperform organic PCM under pulses up to 20 ms. It can be said that under these conditions, thermal conductivity is the dominant property because it allows the PCM to have a more uniform temperature distribution into itself and therefore, when it reaches the melting temperature, it allows a uniform melting. **Figure 6** compares the performance of erythritol, which has a high latent heat of fusion, but low thermal conductivity and Bi/Pb/Sn/In, which has high thermal conductivity but lower latent heat of fusion than erythritol. For this comparison, a 20 J pulse from 1 ms up to 10 seconds were used, and assuming same dimensions and thickness of the heat source and PCM previously used. Due to the difference on melting temperature of erythritol (117°C) and Bi/Pb/Sn/In (57°C), the ambient temperature was fixed as 20°C less than their melting temperature ($T_{amb} = T_{melt} - 20^{\circ}C$). The temperature benefit, described in equation (13), was used to compare the performance of both materials.

$$T.B. = T_{max} - T_{\infty} \quad (13)$$

As it can be seen in **Figure 7**, a significant benefit can be obtained by using metallic PCM for short pulses, as 1 ms where an 80°C difference between the metallic PCM and organic PCM is shown. However, the thermal benefit of using metallic PCM decrease with longer pulse. At 1s pulse the benefit of metallic over organic is virtually inexistence. At this point, the complexity, cost and weight on metallic PCMs could became a driving decision factor in whether to use metallic or organic PCM.

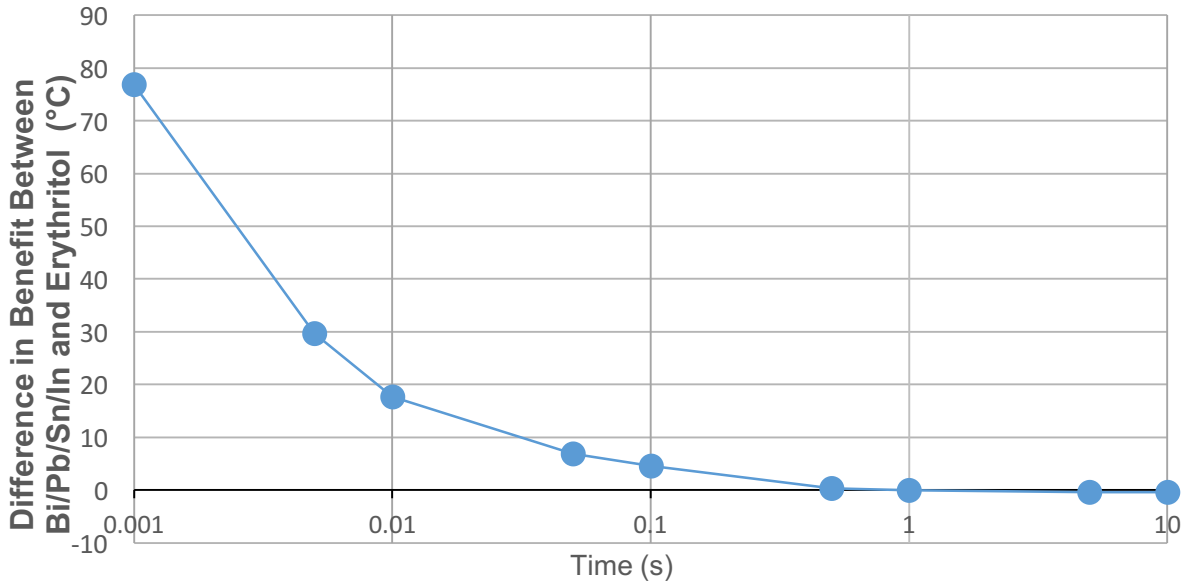


Figure 7: Comparison of using a metallic PCM (Bi/Pb/Sn/In) and an organic PCM (erythritol) at same energy pulse but different length.

4.1.4 CONCLUSION

A 1-D heat transfer analysis was done, using finite-difference method and heat integration method to model the heat transfer and the melting process, respectively. Under this study, it was assumed a flat square as the heat source and 0.1016mm of PCM directly on top of the heat source. Different pulse conditions were used, consisting on high power short pulses, to study the performance of each PCM and were compared to a silicone dielectric gel.

Metallic PCMs outperformed organic PCM during high power short pulses. However, the model shows that the benefit of using metallic PCMs decreases at pulses $>.1s$ at the studied condition.

The model developed in this work demonstrates that it could be used as a valuable designing tool. This model can be used as guide on the choosing of the appropriate PCM on the appropriate pulse condition.

4.2 HEATER/RTD

One of the most challenging issues in this experiment is the temperature measurement at the milliseconds time scale. The use of traditional measurement methods has the drawback of thermal response and thermal contact area. In this experiment, a flat chip is used as heater, where PCM is poured directly on top. If a thermocouple, which has a sphere like sensor, is used to measure the temperature of the chip, we would have a contact challenge between the heat source and the temperature sensor. As shown in **Figure 8** if we place a sphere sensor on top of a flat surface, the contact between the heat source and the sensor is minimal, resulting in an inaccurate measurement of temperature at the heat source. To improve the temperature measurement, at the heat source, a device with a micro temperature sensor embedded in a heater was designed and fabricated. A resistance temperature detector (RTD) was patterned, along with a heater, in a borosilicate substrate, which with the low thermal conductivity will help us to provide the highest heat with the lowest power possible.

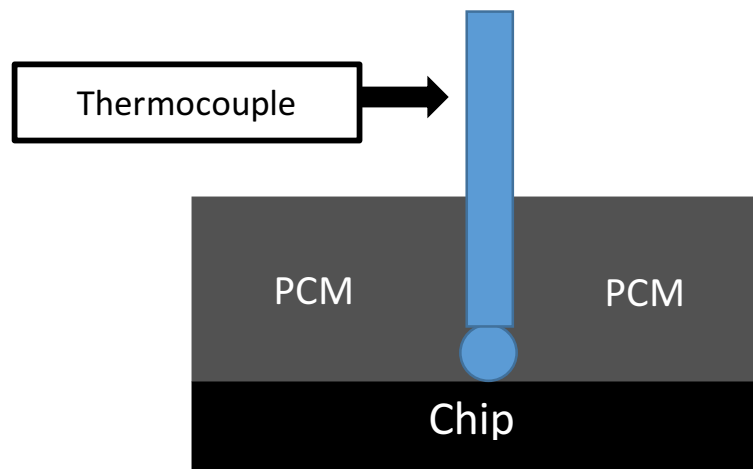


Figure 8: A visual illustration of the challenge of using a thermocouple on a flat surface.

4.2.1 DESIGN

Previously, micro-sensors and nano-sensors have been successfully build in substrate to be able to measure temperature without any invasive techniques and also being able to measure temperature in short time scale [34, 35, 36, 37]. A RTD is a resistive element which its resistance value is temperature sensitive [38], allowing us to track the temperature by measuring the resistance value. For this, a material with a high temperature coefficient of resistance (TCR) is desired because will produce the biggest electrical resistance variability due to temperature which translate in a higher temperature resolution as described in (Equation 14). Copper was chosen as the material for the temperature sensor and heater. Along the high TCR of copper [$\alpha=0.004/^{\circ}\text{C}$], which will bring high temperature resolution in our temperature sensor, fabrication simplicity's sake was taken in the consideration for the material selection.

$$R = R_{\text{ref}}[1 + \alpha(\Delta T)] \quad (14)$$

Using the same material for both component we can fabricate them at the same time by one metallization. The main disadvantage of using a high TCR material for the heater is the variability of electrical resistance due to temperature. Power dissipation can be described by the equation (15), where V is volt and R is resistance. If the heater has a resistance varying due to temperature, the power will also vary due to temperature, which can affect the comparison of two materials. However, the change in power could also be used as a performance measurement. A material that is able to absorb more energy, therefore able to maintain the device at lower temperature, will have the lowest change in power.

$$P = \frac{V}{R} \quad (15)$$

Equation 16, where ρ and L are the material's resistivity and length respectively and w and t are the wide and the thickness of the material respectively, was used to choose the dimensions of the RTD and heater. To achieve a high power with low voltage, the heater need to have a low resistance, however, the temperature sensor need to have the highest resistance possible to have the highest temperature resolution. Since the RTD and heater will be done by the same material, one copper deposition will be made, therefore, the same thickness for both components is assumed. To achieve a different resistance values between the heater and the RTD, different width was chosen for both. The heater has a wider pathway than the RTD. To create a heater that would produce a uniform temperature thru all the device, it was decided to design the heater using a serpentine shape that covers most of the surface area of the device. The RTD was placed very near, surrounding the heater's pathway in order to capture the most accurate temperature possible. After a schematic design was chosen, a heat transfer analysis, varying the dimensions was done.

$$R = \frac{\rho L}{wt} \quad (16)$$

ANSYS was used to perform heat transfer analysis varying the width of the heater's trace and the spacing between them. Producing a uniform temperature thru all surface, in a borosilicate substrate, which has low thermal conductivity, could be challenging. It was studied the effect of spacing between of heater's pathway and the width of the heater pathway. With larger spacing or wider pathways, a more temperature

gradient is obtained thru the substrate; however, because the need of having a low electrical resistance in the heater, a trade-off between the temperature gradient and the resistance value was done. **Figure 9** shows the final design and **Table 3** shows the final dimensions.

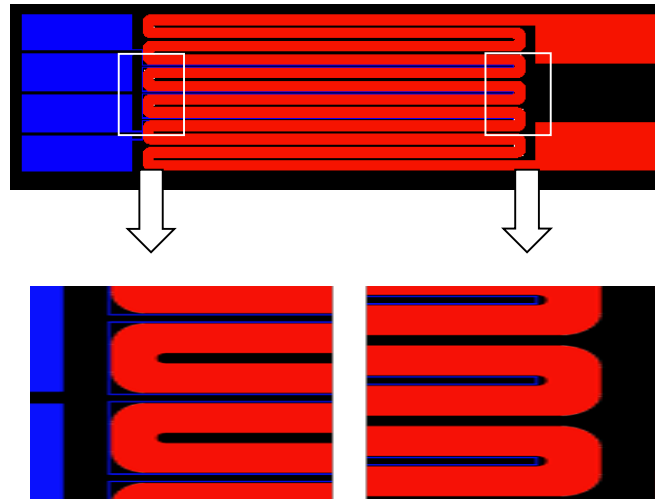


Figure 9: Illustration of the final design. In blue (thin lines) is shown the RTD and in red (thick lines) the heater.

Table 3: Final dimensions for the heater/RTD device.

Pathway		
	Heater	RTD
Width (mm)	0.280	0.010
Spacing		
	From heater to RTD	From heater to heater
Width (mm)	0.010	0.100
Thickness		
	Heater	RTD
Thickness (μm)	0.550	0.550
Heat Source Area		
Length (mm)	Wide (mm)	
10.5	4.5	

4.2.2 FABRICATION

Traditional micro-fabrication processes were used to fabricate the devices. First, the mask was designed using a computer software (DraftSight). Then, a direct laser writer was used to make the mask. Two masks were fabricated for the fabrication of the device, one for the heater/RTD and the other one for the silicon nitride.

Lift-off process was used to fabricate the device. The heater and RTD were done by sputtered copper, while the silicon nitride was deposited via plasma enhanced chemical vapor deposition (PECVD). A thin layer of Titanium was used as adhesion layer for the copper and gold was deposited, on top of the heater and RTD connection pads as oxidation protection layer, via thermal evaporation. The fabricated device is shown in

Figure 10

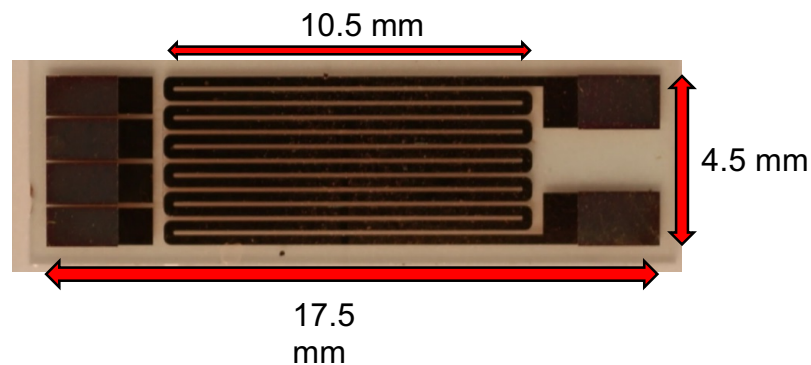


Figure 10: A sample of a fabricated device.

4.2.3 PACKAGING

A commercial ceramic leaded package was used to extend the RTD and heater connection. **Figure 11** shows a digital representation of how the device should look like. **Figure 12** shows the sequence to build the package to be used on the experiment. First, the RTD/Heater was attached to the package and the device was wire bonded to the

package. Then, not shown in the figure, the device was calibrated. After the device was calibrated, a container, that was manufactured using additive manufacturing technique, was attached on top of the heat source. It was ensure that the container was well attached to the device, otherwise spillage of any liquid material could occur. At last, the selected material to be used, was poured inside of the container.

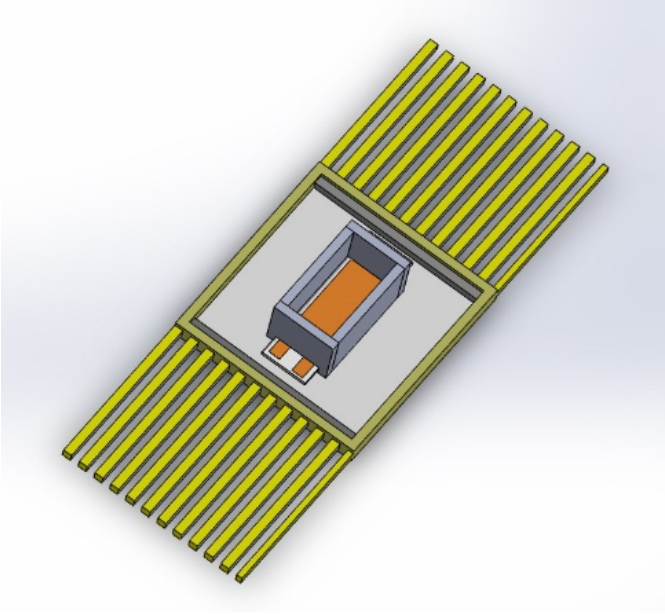


Figure 11: Digital representation of the final device with the plastic PCM container.

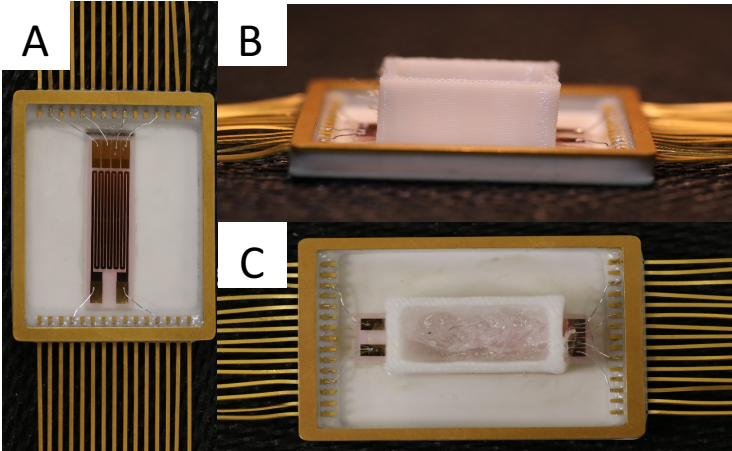


Figure 12: Sequence of the package preparation.

4.2.4 CALIBRATION

A temperature/resistance calibration is done to make a correlation between the temperature and the resistance of the temperature sensor. To perform the calibration, a thermocouple was attached to the device. The device was placed inside of a furnace. The furnace was set to a desired temperature. Once the temperature was stable on the device, which is monitored by the thermocouple, the temperature was recorded along the resistance. This procedure was done at different temperatures. All devices showed a good resistance-temperature correlation. A linear fit was performed on each calibration curve and the resolution of each device were around $1.5^{\circ}\text{C}/\Omega - 2^{\circ}\text{C}/\Omega$. The **Figure 13** shows an example of the calibration of three devices and **Table 4** shows the numerical calibration data for same three devices. Refers to the **Appendix A** to more calibration curves and numerical data.

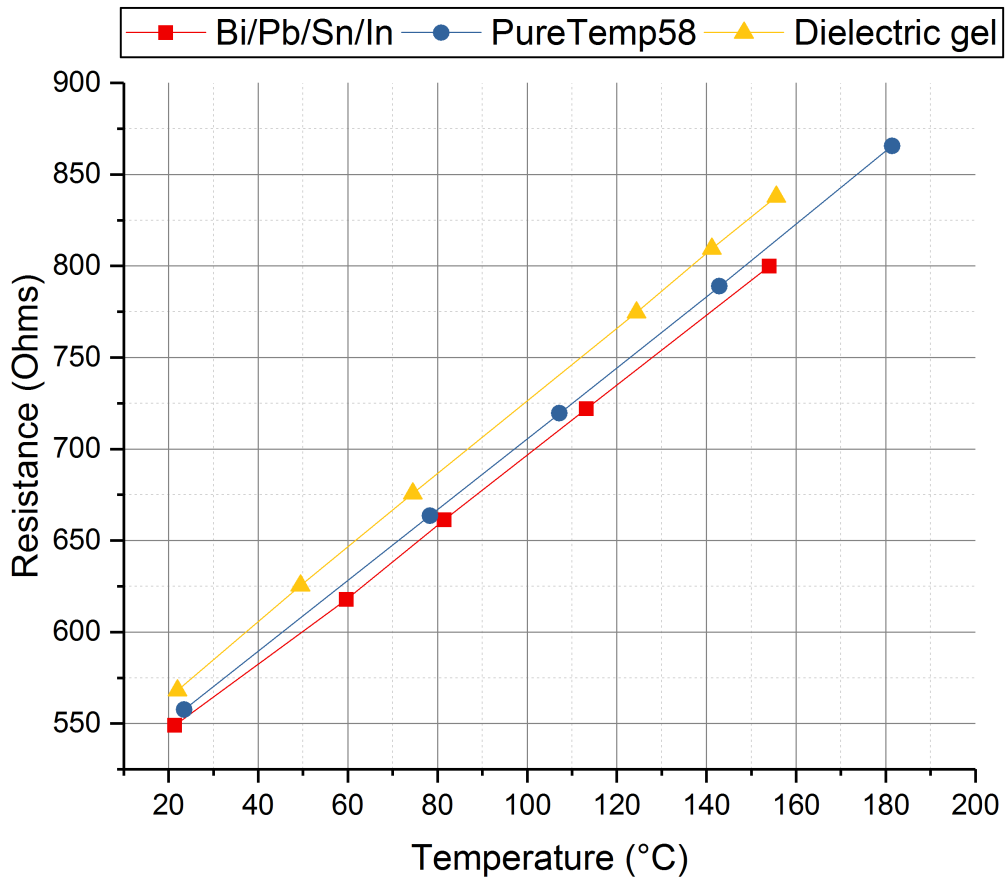


Figure 13: Temperature - resistance calibration curve of three different devices.

Table 4: Numerical calibration data of three devices.

Bi/Pb/Sn/In		Dielectric Gel		PureTemp58x	
Temperature (°C)	Resistance (Ω)	Temperature (°C)	Resistance (Ω)	Temperature (°C)	Resistance (Ω)
21.4	549.1	22	568.1	23.5	557.7
59.7	617.8	49.4	625.4	78.3	663.6
81.5	661.3	74.5	675.7	107.2	719.5
113.2	722.1	124.4	774.7	142.9	788.9
154	799.9	141.2	809.5	181.4	865.6

4.2.5 TEST

Once the devices were calibrated, they were tested without any material on top to ensure the quality of each device. A 31 W and near to 20ms pulse were done on each device to be used. It was expected that all devices perform similar because they were fabricated at the same time. With this test, it was ensured that the heater and RTD were working properly. **Figure 14** shows the performance of two devices at 31 W pulse without any material on top. Both devices have a similar performance, which means that both devices are acceptable to be used for high power pulses. Same tests were done with all devices and similar results were obtained. This test demonstrate that devices are capable of making a pulse and monitor the temperature at the milliseconds time scale, also that all devices used in this research are similar. Refers to the **Appendix B** for result of others devices.

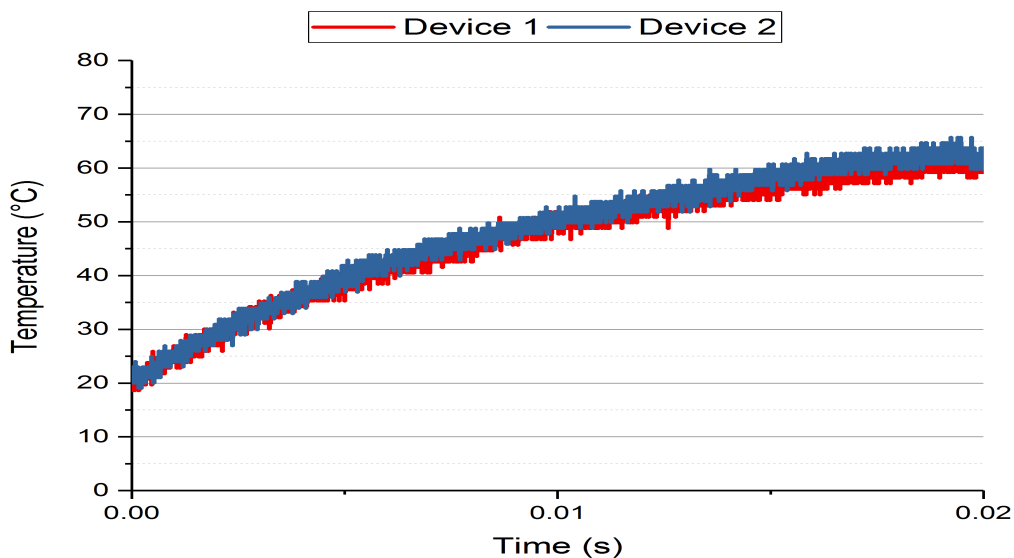


Figure 14: Result of two devices pulsed with a 31W and near to 20 ms pulse without any PCM or encapsulant on top.

4.2.6 CONCLUSION

In this chapter, a description of the device used to perform the high-power pulse experiment, is presented. The device was designed with the scope of having a device that represent a real device, but with an integrated temperature sensor capable of measuring temperature at the milliseconds time scale. Also, this device needed to withstand liquid metal on top, without suffering any damage.

The fabricated devices showed a good liner relationship between resistance and temperature, which makes possible to use it as temperature sensor. The tests performed on the devices also showed that the devices could be used to heat and monitor the temperature at the millisecond time scale. The development of this novel devices could lead to more accurate studies on performance of different cooling systems, especially on the milliseconds pulse experiments.

4.3 HIGH POWER PULSE EXPERIMENT

In **section 4.1**, it was discussed how metallic PCMs should perform better than organic PCMs during high-power short pulses via numerical evaluation. To confirm the results obtained in **section 4.1** a device capable to heat and monitor the temperature during at all time, was fabricated and explained in **section 4.2**. The scope of this chapter is to confirm, via experimentation, what the numerical evaluation suggested.

After the device described in **section 4.2** were calibrated and tested, they were filled with different materials at the thickness (2mm). Two metallic PCMs were used (49Bi/18Pb/12Sn/21In and Fields' Metal); two commercially available organic PCMs (Pure Temp 29x and PureTemp 58x) and a dielectric gel were used as baseline to compare the performance of metallic PCMs. **Table 5** shows material used during the experiment and their respective properties. Each device were tested with one pulse of $\approx 19\text{ms}$ at different power ranging from 40W up to 160W.

Table 5: List of material used during experiment and their properties.

Material	T_m ($^{\circ}\text{C}$)	ρ (kg/m^3)	k ($\text{W}/(\text{m}\cdot\text{K})$)	c_p ($\text{kJ}/(\text{kg}\cdot\text{K})$)	H (kJ/kg)	Ref.
Fields' Metal	59			0.250		[39]
Bi/Pb/Sn/In	58	9010	33.2	0.323	28.9	[23,27]
PureTemp29	29	940	0.25	1.77	202	[40]
PureTemp58	58	890	0.25	2.47	225	[41]
Sylgard 527	N/A					

4.3.1 EXPERIMENT PROCEDURE

An in lab-fabricated capacitor bank of 800 μ F was used to make the power pulses. The capacitor bank was provided by the U.S. Army Research Laboratory. The design details will not be discussed. This capacitor bank can make an almost square or constant power pulse at the milliseconds time scale.

A process diagram of the experimental procedure is shown in **Figure 15**. First, the capacitor bank is charged by a power supply up to the desired power and the RTD is powered, using 1mA of current, by the power supply Keysight U3606B. Then, the capacitor bank is discharged by triggering it using a function generator (Agilent 33250A Waveform Generator). While the capacitor bank is discharging, the heater will start to heat and the RTD will be measuring the temperature. The voltage and current input from the capacitor bank to the heater are measured using the Probe Master (High Voltage Differential Probe) and Tektronix TCPA 300 Amplifier AC/DC Current Probe respectively. From the RTD the voltage is measured using the Hameg HZ109 differential probe. The resistance from the RTD is calculated, using Ohms Law, assuming a constant 1mA current from the power supply and the measured voltage.

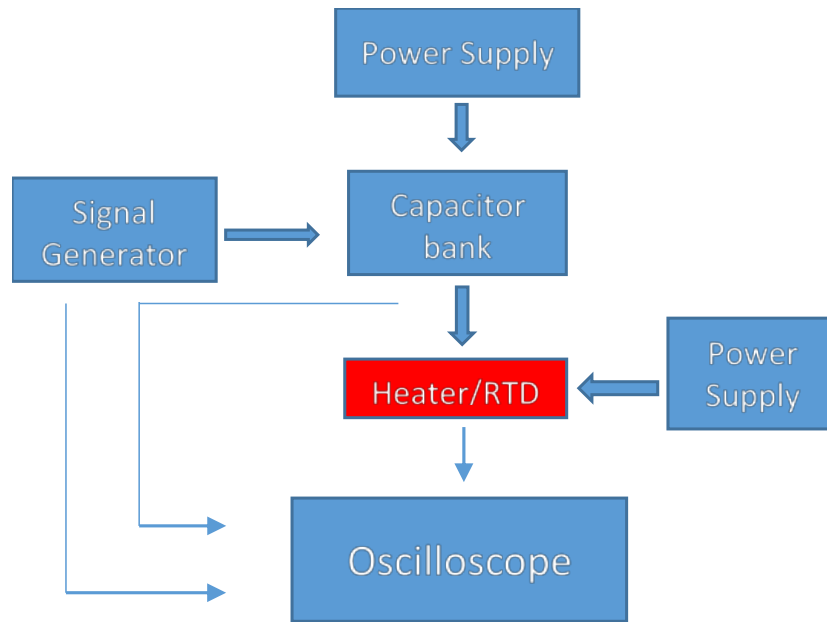


Figure 15: Process diagram on how the experiment is done.

4.3.2 RESULTS AND DISCUSSION

Figure 16 A shows the results from the test done under pulse of 40W. Under this condition, metallic PCMs shows the best performance showing a maximum temperature of 36°C and 43°C for Fields' Metal and Bi/Pb/Sn/In respectively; dielectric gel has the worst performance with a maximum temperature of 57°C. **Figure 16 B** shows the performance of the materials subjected to an 80W pulse. Under this condition, the best performers were Fields' metal and Bi/Pb/Sn/In with a maximum temperature of 49°C and 55°C respectively; the dielectric gel was the worst performance with a maximum temperature of 90°C. Organic PCMs performed similar to dielectric gel on both conditions. Both organic PCMs, having reached their melting temperature, did not perform as well as metallic PCMs. This was expected since it was previously observed in [23] and during the numerical evaluation.

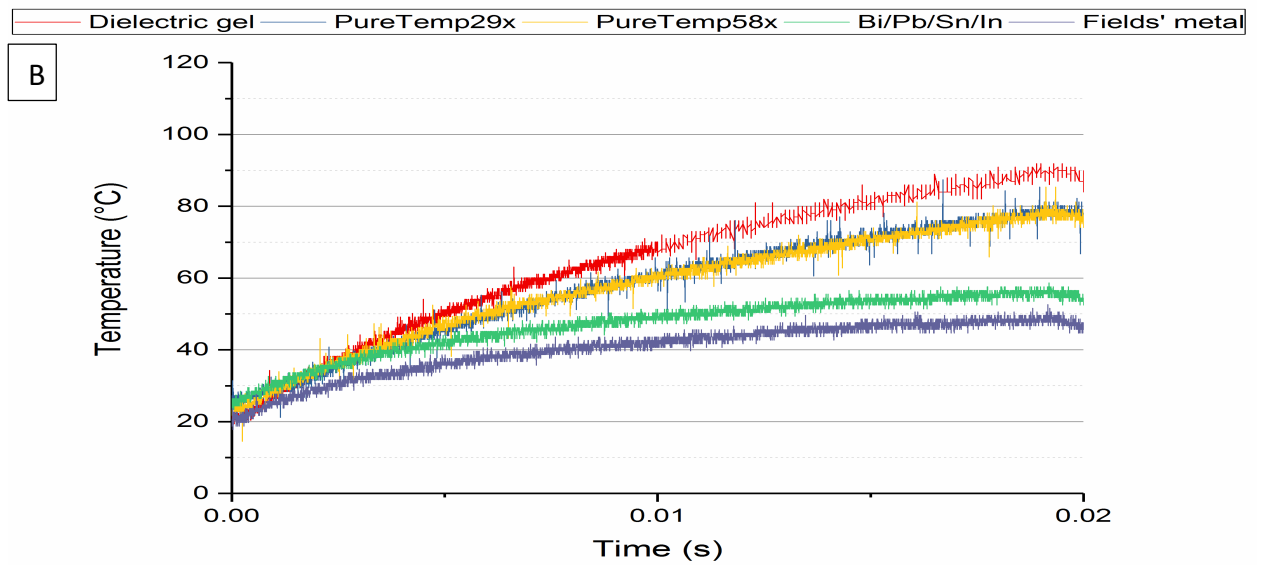
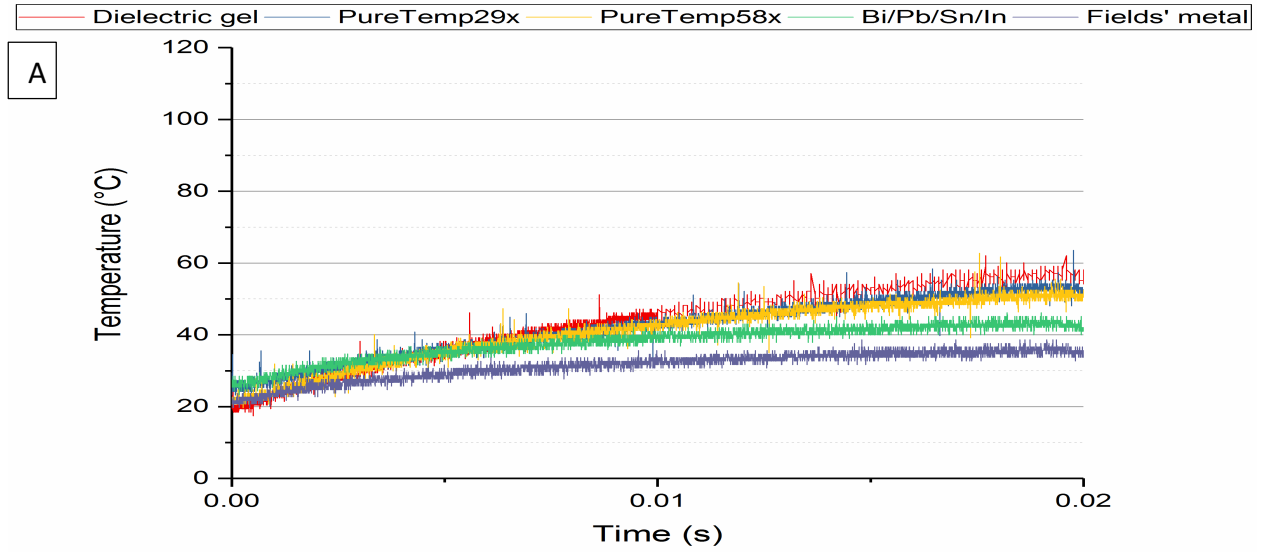


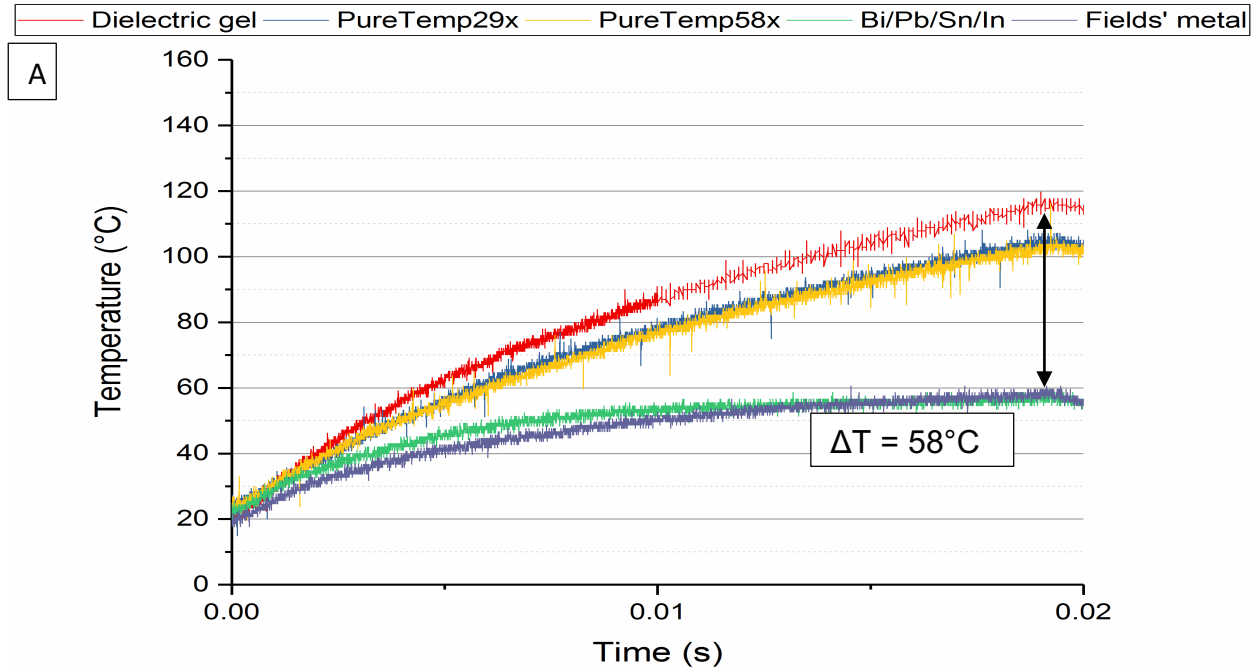
Figure 16: Performance of different materials subjected to a high power short pulses. A) Result from a pulse of 40W. B) Results from a pulse of 80W.

Table 6: Numerical data from Figure 16

Material	Minimum (°C)	Maximum (°C)	ΔT (°C)	%difference compared to dielectric gel.
40 W				
Fields' metal	22	36	14	62
Bi/Pb/Sn/In	26	43	17	54
PureTemp-29	25	53	28	24
PureTemp-58	22	52	30	19
Dielectric	20	57	37	
80 W				
Fields' metal	22	49	27	61
Bi/Pb/Sn/In	25	55	30	56
PureTemp-29	27	79	52	25
PureTemp-58	24	78	54	22
Dielectric	21	90	69	

Figure 17 A shows the materials performance under a 120W. Metallic PCMs were the best performers with a maximum temperature of 58°C (Bi/Pb/Sn/In) and 59 °C (Fields' metal). An improvement of 58°C was seen when it is compared to dielectric gel, also metallic PCMs were able to maintain a temperature increment >60% lower than dielectric gel. Under this condition, metallic PCMs reached their melting point. For the Bi/Pb/Sn/In it can be seen a plateau behavior which suggest that the material reached it melting temperature. Under 160W pulse, shown in **Figure 17 B** it become clearer the plateau behavior near to the melting temperature, suggesting that a phase transformation is occurring. Bi/Pb/Sn/In, at 160W pulse, was able to maintain a temperature increment 68.4% lower than dielectric gel. A difference on maximum temperature of 80°C was achieved when metallic PCM is implemented instead of dielectric gel. Bi/Pb/Sn/In reached its melting temperature near to 5ms and from that point until the end of the pulse, the metallic PCM was able to manage an increment of 5°C - 6°C, while the dielectric gel have

an increment of 65°C. In **Figure 17 C**, can be seen how Fields' metal outperformed dielectric gel by a temperature difference of 125°C.



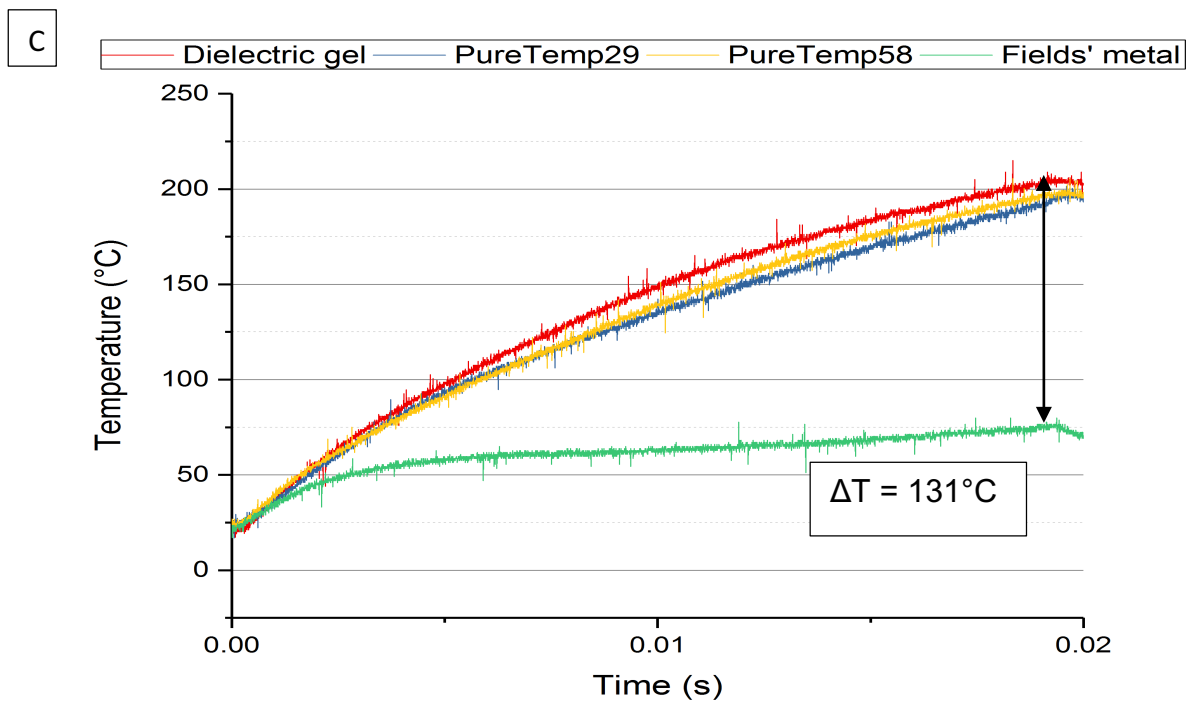
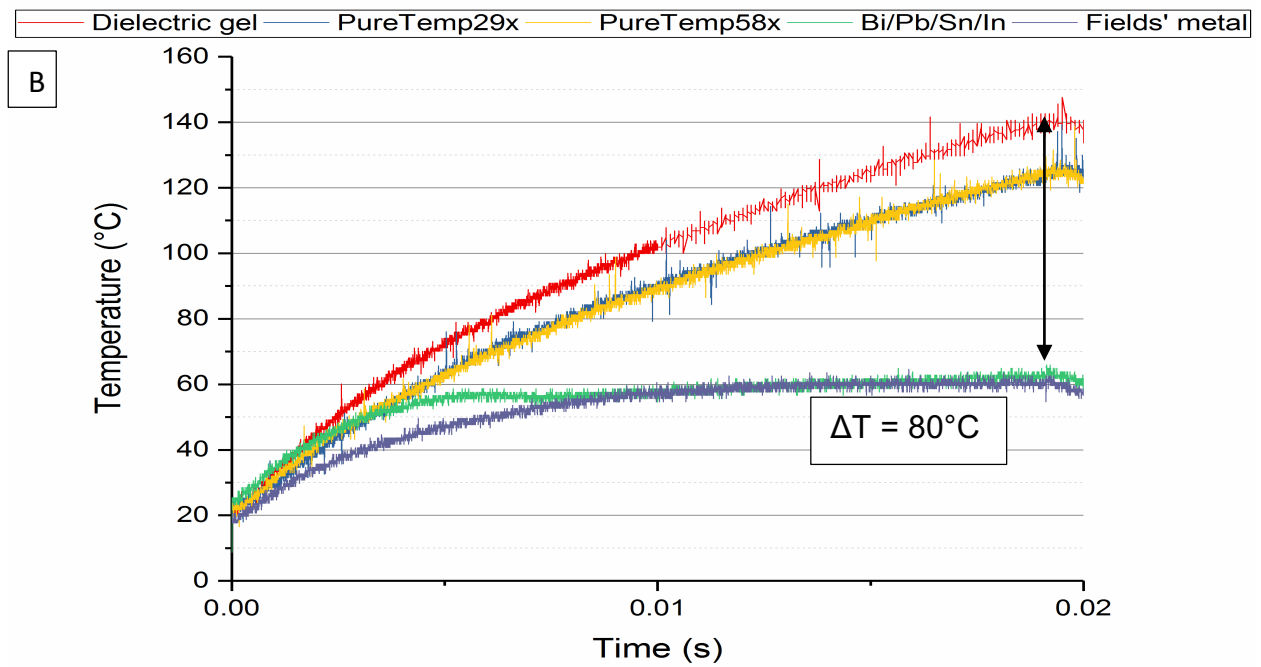


Figure 17: Performance of different materials subjected to a high power short pulses. A) Result from a pulse of 120 W. B) Results from a pulse of 160 W C) Results from a pulse of 280 W..

Table 7: Numerical data from Figure 17

Material	Minimum (°C)	Maximum (°C)	ΔT (°C)	%difference compared to dielectric gel.
120 W				
Fields' metal	21	59	38	60
Bi/Pb/Sn/In	23	58	35	63
PureTemp-29	25	105	80	16
PureTemp-58	24	103	79	17
Dielectric	21	116	95	
160 W				
Fields' metal	20	61	41	66
Bi/Pb/Sn/In	25	63	38	68
PureTemp-29	23	126	103	13
PureTemp-58	23	125	102	14
Dielectric	22	141	119	
280 W				
Fields' metal	23	75	52	72
Bi/Pb/Sn/In	Due to technical problems, this alloy was not tested at this condition.			
PureTemp-29	23	200	177	4
PureTemp-58	24	200	176	4
Dielectric	22	205	183	

Figure 18 shows the thermal benefit, $T_{\max, \text{PureTemp58}} - T_{\max, \text{Bi/Pb/Sn/In}}$, of using metallic PCM (Bi/Pb/Sn/In) over organic PCM (PureTemp58x). The metallic PCM overcame organic PCM over all conditions, however, the benefit increase while the power input is increased. This trend, of benefit of using metallic PCM over organic PCM was also seen in **Figure 7**, where the model suggests that the benefit of using metallic PCM, over organic PCM, would increase while increasing the power. This benefit of using metallic PCM under high power pulses puts metallic PCM as a potential thermal solution for transient application. This benefit could be bigger if the difference in power input, due to the power drop related to the change in resistance in the heater, is considered.

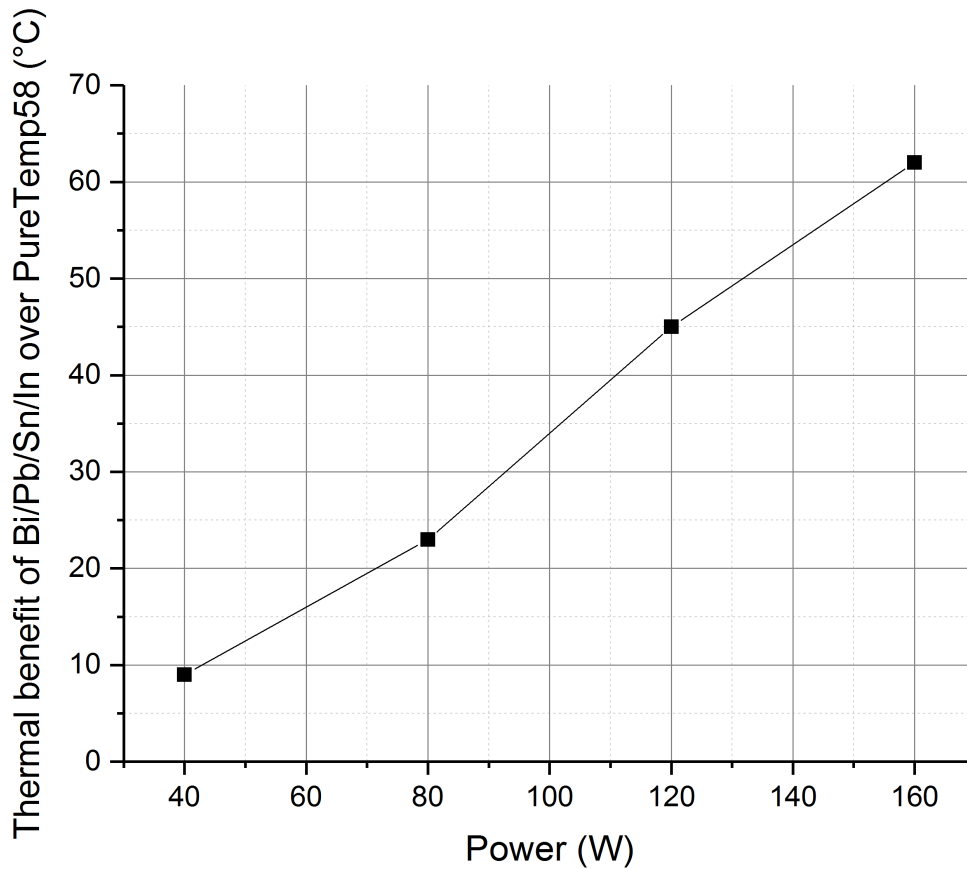


Figure 18: Thermal benefit of using Bi/Pb/Sn/In over PureTemp 58x.

As it was discussed before, the heater is made of copper which has a high TCR. Having a material that change it resistance due to temperature, in this case increase, will make the power to decrease when temperature is increasing. **Figure 19** shows how the power input, for Bi/Pb/Sn/In and Dielectric gel for 160W pulse, vary thru the time. This variation is due to the capacitor discharging and also the temperature increase at the device. It can be seen that at near to 5ms, the power input to the dielectric gel start to lower at faster rate than the power input to Bi/Pb/Sn/In. This coincide with Bi/Pb/Sn/In reaching its melting temperature, therefore can be said that a major difference in temperature between the dielectric gel and the metallic PCM is causing this difference in

power input. The lowest power input level of the metallic PCM was around 115W, while the dielectric gel was 85W. Taking in consideration the difference in power input, we can infer that performance of metallic PCMs could be even greater than previously shown. Please refer to **Appendix C – F**, for more power inputs plots.

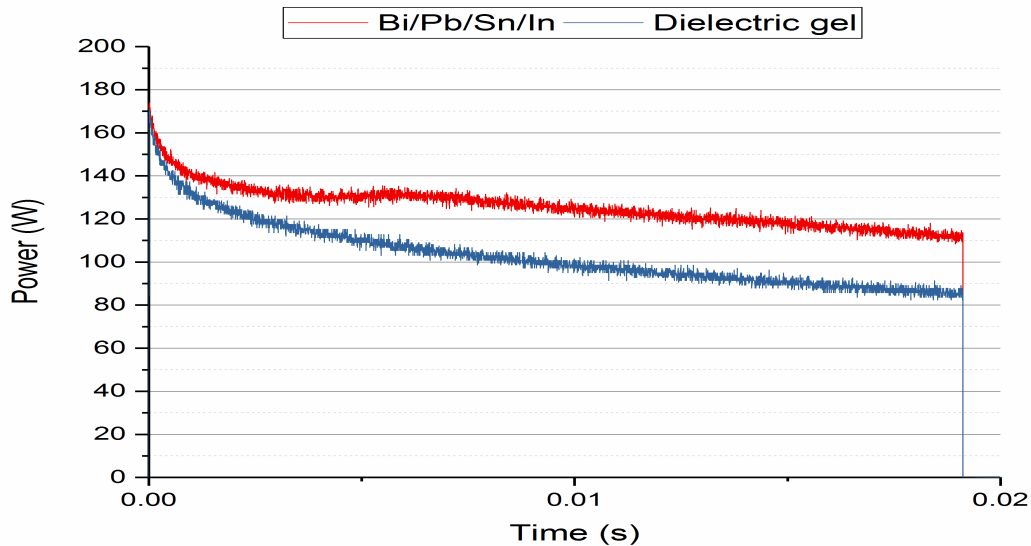


Figure 19: Power input thru time of Bi/Pb/Sn/In and dielectric gel.

4.3.3 CONCLUSION

An experimental evaluation of metallic PCM, organic PCM and a dielectric gel were done under ≈ 20 ms pulses ranging from 40W up to 160W. Metallic PCMs outperformed organic PCM and dielectric gel under all studied conditions.

Under 160W pulse, a temperature plateau behavior was seen for metallic PCMs. Bi/Pb/Sn/In was able to hold temperature from rise, allowing a temperature increment of around 5°C during 75% of the pulse time; meanwhile, dielectric gel allowed a temperature increment of 65°C , 1200% what the metallic PCM allowed. The results obtained during this investigation, make a no-doubter, the ability of metallic PCM to suppress high

temperature peak; making them an ideal passive cooling system for transient applications.

5. CONCLUSION

The main objective behind this thesis was to evaluate the performance of metallic PCMs to act as thermal buffer for pulse power applications. The performance was evaluated, first numerically via a 1-D numerical method and then experimentally. For the experimental evaluation, a heater/RTD device was fabricated using traditional micro-fabrication processes.

This thesis produced a simple 1-D numerical model which can be used as tool to perform a quick material evaluation as potential thermal buffer passive cooling system. The model showed that metallic PCMs outperform organic PCMs under high heat flux short pulses, which the result was validated later via experimental evaluations. Also, this model suggests that thermal conductivity could dominate the performance under high heat flux pulses, but latent heat of fusion is the dominant property under, same energy but wider pulses.

A unique device was developed that work as heater and temperature sensor. This device, showed that can measure the junction temperature at the milliseconds time scale. This is a novel device that can be used as a tool to evaluate the performance of any other electronic cooling system. The fabricated device was used to perform the experimental evaluation of different PCMs.

The experimental evaluation validates what the numerical model suggested. The metallic PCMs outperformed the organic PCMs under high heat flux short pulses and could make a thermal suppression during such pulses. A difference up to 80°C was seen when replacing dielectric gel by a metallic PCM.

During this work, it was demonstrated, numerically and experimentally, the viability of using metallic PCMs as passive cooling system for pulse power applications.

6. REFERENCE

- 1 Moore, G. (1965). Cramming more components onto integrated circuits, *Electronics*, vol. 38. Apr, 19, 114-117.
- 2 Choi, U. M., Blaabjerg, F., & Lee, K. B. (2015). Study and handling methods of power IGBT module failures in power electronic converter systems. *Power Electronics, IEEE Transactions on*, 30(5), 2517-2533. doi: 10.1109/TPEL.2014.2373390
- 3 Ramshaw, E. (2013). Transient Thermal Impedance. In E. Ramshaw, *Power Electronics Semiconductor Switches* (pp. 222-225). Springer Science & Business Media.
- 4 Meysenc, L., Jylhakallio, M., & Barbosa, P. (2005). Power electronics cooling effectiveness versus thermal inertia. *IEEE Transactions on Power Electronics*, 20(3), 687-693. doi: 10.1109/TPEL.2005.846548
- 5 Jankowski, N. R., Morgan, B. C., & McCluskey, F. P. (2009, January). Design and fabrication of a substrate integrated phase change thermal buffer heat sink. In *ASME 2009 International Mechanical Engineering Congress and Exposition* (pp. 75-84). American Society of Mechanical Engineers. doi:10.1115/IMECE2009-12713.
- 6 Soupremanien, U., Szabolics, H., Quenard, S., Bouchut, P., Roumanie, M., Bottazzini, R., & Dunoyer, N. (2016, May). Integration of metallic phase change material in power electronics. In *Thermal and Thermomechanical Phenomena in Electronic Systems (ITherm), 2016 15th IEEE Intersociety Conference on* (pp. 125-133). IEEE. doi: 10.1109/ITHERM.2016.7517539
- 7 Hale, D. V., Hoover, M. J., & O'Neill, M. J. (1971). Phasechange materials handbook. Technical Report. Huntsville (AL): National Aeronautics and Space Administration; 1971 Sep. Report No.: NASA-CR- 61363. Contract No.: NAS8-25183. doi: 2060/19720012306
- 8 Krishnan, S., & Garimella, S. V. (2003, January). Thermal Management of Transient Power Spikes in Electronics: Phase Change Energy Storage or Copper Heat Sinks??. In *ASME 2003 International Electronic Packaging Technical Conference and Exhibition* (pp. 363-374). American Society of Mechanical Engineers. doi:10.1115/IPACK2003-35169
- 9 Setoh, G., Tan, F. L., & Fok, S. C. (2010). Experimental studies on the use of a phase change material for cooling mobile phones. *International Communications in Heat and Mass Transfer*, 37(9), 1403-1410. <http://dx.doi.org/10.1016/j.icheatmasstransfer.2010.07.013>.
- 10 Chukwu, S., Ogbonnaya, E., & Weiss, L. (2012, July). Fabrication, Testing, and Enhancement of a Thermal Energy Storage Device Utilizing Phase Change Materials. In *ASME 2012 Heat Transfer Summer Conference collocated with the ASME 2012 Fluids*

Engineering Division Summer Meeting and the ASME 2012 10th International Conference on Nanochannels, Microchannels, and Minichannels (pp. 279-285). American Society of Mechanical Engineers. doi:10.1115/HT2012-58309

11 Zhao, C. Y., Lu, W., & Tian, Y. (2010). Heat transfer enhancement for thermal energy storage using metal foams embedded within phase change materials (PCMs). *Solar Energy*, 84(8), 1402-1412. <http://dx.doi.org/10.1016/j.solener.2010.04.022>.

12 Fleischer, A. S., Chintakrinda, K., Weinstein, R., & Bessel, C. A. (2008, May). Transient thermal management using phase change materials with embedded graphite nanofibers for systems with high power requirements. In *Thermal and Thermomechanical Phenomena in Electronic Systems, 2008. ITherm 2008. 11th Intersociety Conference on* (pp. 561-566). IEEE.

13 Mahmoud, S., Tang, A., Toh, C., Raya, A. D., & Soo, S. L. (2013). Experimental investigation of inserts configurations and PCM type on the thermal performance of PCM based heat sinks. *Applied Energy*, 112, 1349-1356

14 Xie, B., Cheng, W. L., & Xu, Z. M. (2015). Studies on the effect of shape-stabilized PCM filled aluminum honeycomb composite material on thermal control. *International Journal of Heat and Mass Transfer*, 91, 135-143.

15 Krishnan, S., & Garimella, S. V. (2003, January). Thermal Management of Transient Power Spikes in Electronics: Phase Change Energy Storage or Copper Heat Sinks??. In *ASME 2003 International Electronic Packaging Technical Conference and Exhibition* (pp. 363-374). American Society of Mechanical Engineers.

16 Jankowski, N. R., & McCluskey, F. P. (2014). A review of phase change materials for vehicle component thermal buffering. *Applied Energy*, 113, 1525-1561.

17 Ge, H., Li, H., Mei, S., & Liu, J. (2013). Low melting point liquid metal as a new class of phase change material: An emerging frontier in energy area. *Renewable and Sustainable Energy Reviews*, 21, 331-346.

18 Sharma, S. D., Iwata, T., Kitano, H., & Sagara, K. (2005). Thermal performance of a solar cooker based on an evacuated tube solar collector with a PCM storage unit. *Solar Energy*, 78(3), 416-426.

19 Tyagi, V. V., Pandey, A. K., Kaushik, S. C., & Tyagi, S. K. (2012). Thermal performance evaluation of a solar air heater with and without thermal energy storage. *Journal of thermal analysis and calorimetry*, 107(3), 1345-1352.

20 Chung, M. H., & Park, J. C. (2016). Development of PCM cool roof system to control urban heat island considering temperate climatic conditions. *Energy and Buildings*.

- 21 Akeiber, H., Nejat, P., Majid, M. Z. A., Wahid, M. A., Jomehzadeh, F., Famileh, I. Z., ... & Zaki, S. A. (2016). A review on phase change material (PCM) for sustainable passive cooling in building envelopes. *Renewable and Sustainable Energy Reviews*, 60, 1470-1497.
- 22 Shamberger, P. J. (2016). Cooling capacity figure of merit for phase change materials. *Journal of Heat Transfer*, 138(2), 024502. doi:10.1115/1.4031252
- 23 Lei Shao, Arun Raghavan, Gun-Ho Kim, Laurel Emurian, Jeffrey Rosen, Marios C. Papaefthymiou, Thomas F. Wensch, Milo M.K. Martin, Kevin P. Pipe, Figure-of-merit for phase-change materials used in thermal management, *International Journal of Heat and Mass Transfer*, Volume 101, October 2016, Pages 764-771, ISSN 0017-9310, <http://dx.doi.org/10.1016/j.ijheatmasstransfer.2016.05.040>.
- 24 Ge, H., & Liu, J. (2013). Keeping smartphones cool with gallium phase change material. *Journal of Heat Transfer*, 135(5), 054503.
- 25 Ge, H., & Liu, J. (2012). Phase change effect of low melting point metal for an automatic cooling of USB flash memory. *Frontiers in Energy*, 1-3. DOI: 10.1007/s11708-012-0204-z
- 26 Shao, L., Raghavan, A., Emurian, L., Papaefthymiou, M. C., Wensch, T. F., Martin, M. M., & Pipe, K. P. (2014, March). On-chip phase change heat sinks designed for computational sprinting. In *Semiconductor Thermal Measurement and Management Symposium (SEMI-THERM), 2014 30th Annual* (pp. 29-34). IEEE. DOI: [10.1109/SEMI-THERM.2014.6892211](https://doi.org/10.1109/SEMI-THERM.2014.6892211)
- 27 Ai-Gang Pan, Jun-Biao Wang, Xian-Jie Zhang, Xiao-Bao Cao. Experimental Research of Electronic Devices Thermal Control Using Metallic Phase Change Materials[J]. *Journal of Harbin Institute Of Technology (New Series)*, 2014, (2): 113-121. DOI: 10.11916/j.issn.1005-9113.2014.02.017
- 28 Li-Wu Fan, Yu-Yue Wu, Yu-Qi Xiao, Yi Zeng, Yi-Ling Zhang, Zi-Tao Yu, Transient performance of a thermal energy storage-based heat sink using a liquid metal as the phase change material, *Applied Thermal Engineering*, Volume 109, Part A, 25 October 2016, Pages 746-750, ISSN 1359-4311, <http://dx.doi.org/10.1016/j.applthermaleng.2016.08.137>.
- 29 Desai, T. G., Piedra, D., Bonner, R., & Palacios, T. (2012, May). Novel junction level cooling in pulsed GaN devices. In *Thermal and Thermomechanical Phenomena in Electronic Systems (ITherm), 2012 13th IEEE Intersociety Conference on* (pp. 421-427). IEEE. doi: 10.1109/ITHERM.2012.6231461 DOI: [10.1109/ITHERM.2012.6231461](https://doi.org/10.1109/ITHERM.2012.6231461)
- 30 Hu, H., & Argyropoulos, S. A. (1996). Mathematical modelling of solidification and melting: a review. *Modelling and Simulation in Materials Science and Engineering*, 4(4), 371. <https://doi.org/10.1088/0965-0393/4/4/004>

31 Incropera, F. P., DeWitt, D. P., Bergman, T. L., & Lavine. (2006). *Fundamentals of Heat and Mass Transfer*. New York, USA: John Wiley & Sons.

32 Zivkovic, B., & Fujii, I. (2001). An analysis of isothermal phase change of phase change material within rectangular and cylindrical containers. *Solar energy*, 70(1), 51-61. [http://dx.doi.org/10.1016/S0038-092X\(00\)00112-2](http://dx.doi.org/10.1016/S0038-092X(00)00112-2)

33 High Temperature Adhesives and Epoxies, Ceramics, Insulation, Epoxies and Epoxy. (n.d.). Retrieved March 02, 2016, from http://www.cotronics.com/vo/cotr/rm_silicones.htm

34 Baeri, P., Campisano, S. U., Rimini, E., & Zhang, J. P. (1984). Time-resolved temperature measurement of pulsed laser irradiated germanium by thin-film thermocouple. *Applied Physics Letters*, 45(4), 398-400. doi: <http://dx.doi.org/10.1063/1.95234>

35 Zhang, X., Choi, H., Datta, A., & Li, X. (2006). Design, fabrication and characterization of metal embedded thin film thermocouples with various film thicknesses and junction sizes. *Journal of Micromechanics and Microengineering*, 16(5), 900. <https://doi.org/10.1088/0960-1317/16/5/004>

36 Chu, D., Wong, W. K., Goodson, K. E., & Pease, R. F. W. (2003). Transient temperature measurements of resist heating using nanothermocouples. *Journal of Vacuum Science & Technology B*, 21(6), 2985-2989. <http://dx.doi.org/10.1116/1.1624255>

37 Phatthanakun, R., Deekla, P., Pummara, W., Sriphung, C., Pantong, C., & Chomnawang, N. (2012, March). Design and fabrication of thin-film aluminum microheater and nickel temperature sensor. In *Nano/Micro Engineered and Molecular Systems (NEMS), 2012 7th IEEE International Conference on* (pp. 112-115). IEEE.

38 Omega. (2016, 04 19). *RTD: Introduction to Resistance Temperature Detectors*. Retrieved from Omega: <http://www.omega.com/prodinfo/rtd.html>

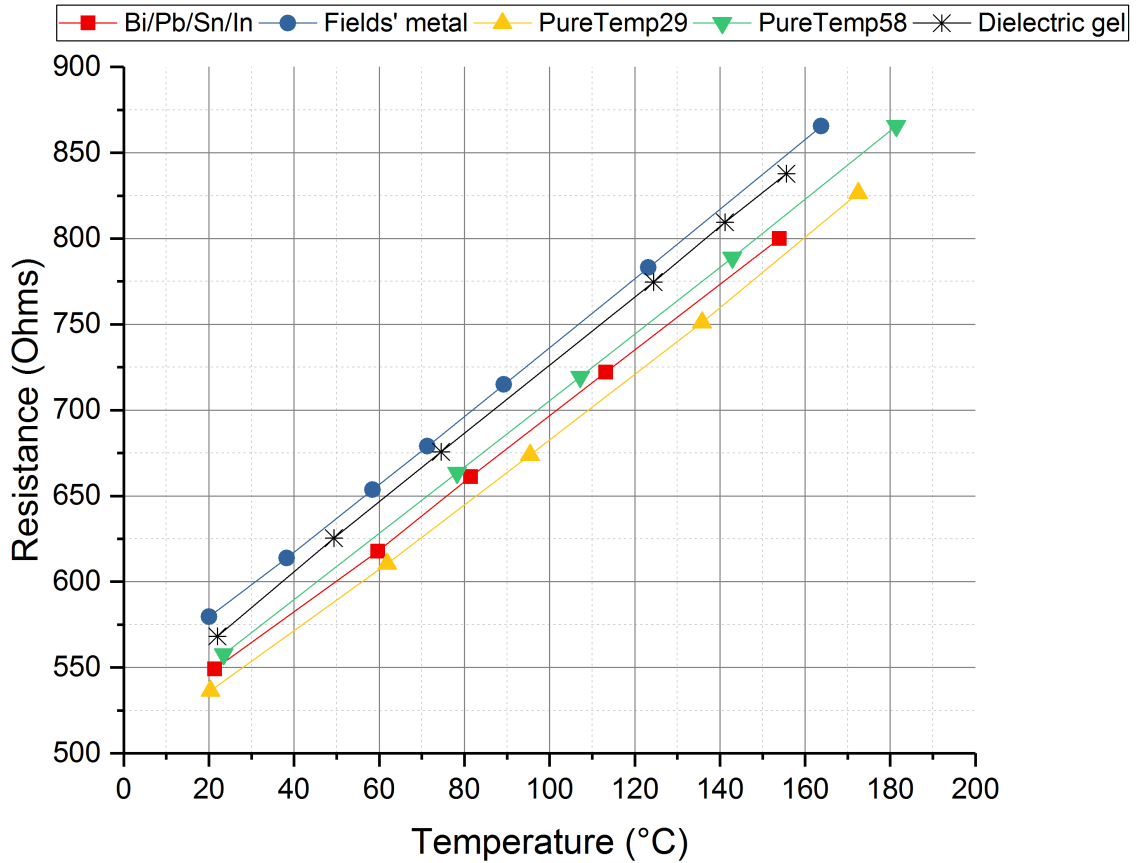
39 Lipchitz, A., Harvel, G., & Sunagawa, T. (2013). Determination of Specific Heat of Eutectic Indium–Bismuth–Tin Liquid Metal Alloys as a Test Material for Liquid Metal-Cooled Applications. *Applied Mechanics and Materials*, 420, 185-193. doi: 10.4028/www.scientific.net/AMM.420.185

40 PureTemp 29 technical data sheet. Retrieved February 16, 2017, from <http://www.puretemp.com/stories/puretemp-29-tds>

41 P. (n.d.). PureTemp 58 technical data sheet. Retrieved February 16, 2017, from <http://www.puretemp.com/stories/puretemp-58-tds>

APPENDIX A

Calibration curves for all devices.



$$\text{Bi/Pb/Sn/In} = y = 1.9233x + 504.97; R^2 = 0.9998$$

$$\text{Fields' metal} = y = 2.0046x + 537.1; R^2 = 0.9999$$

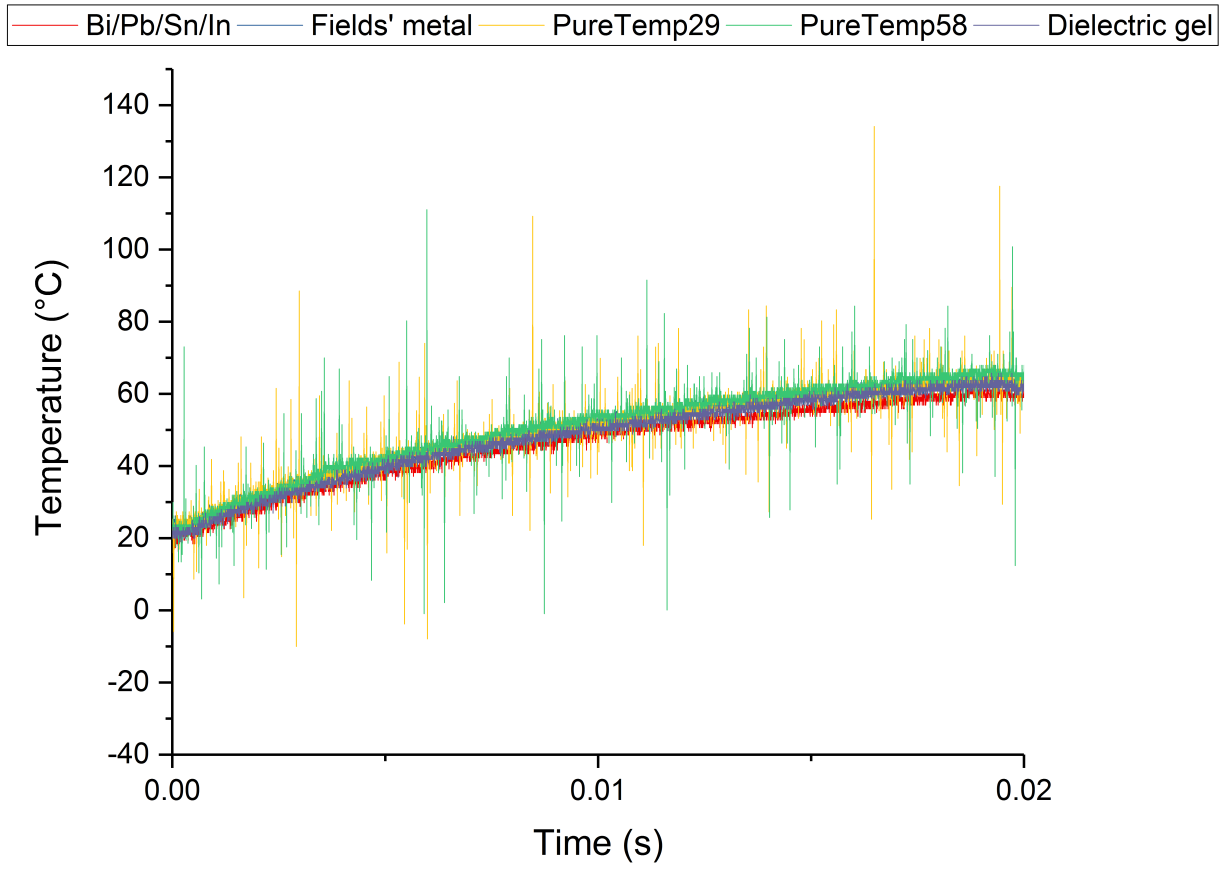
$$\text{PureTemp29} = y = 1.9294x + 492.88; R^2 = 0.9996$$

$$\text{PureTemp58} = y = 1.9473x + 511.4; R^2 = 1$$

$$\text{Dielectric gel} = y = 2.0125x + 524.98; R^2 = 0.9999$$

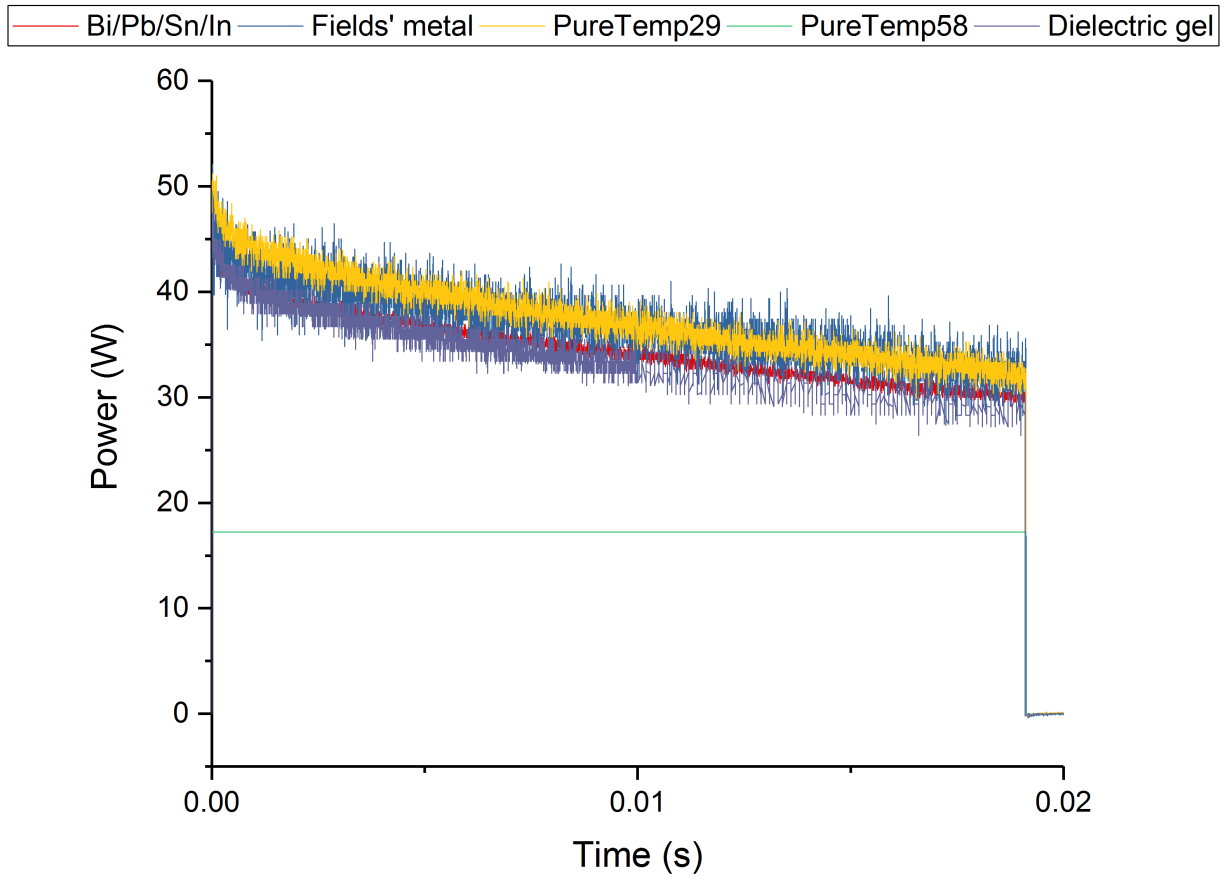
APPENDIX B

Temperature profile of all devices at 31W without PCMs.



APPENDIX C

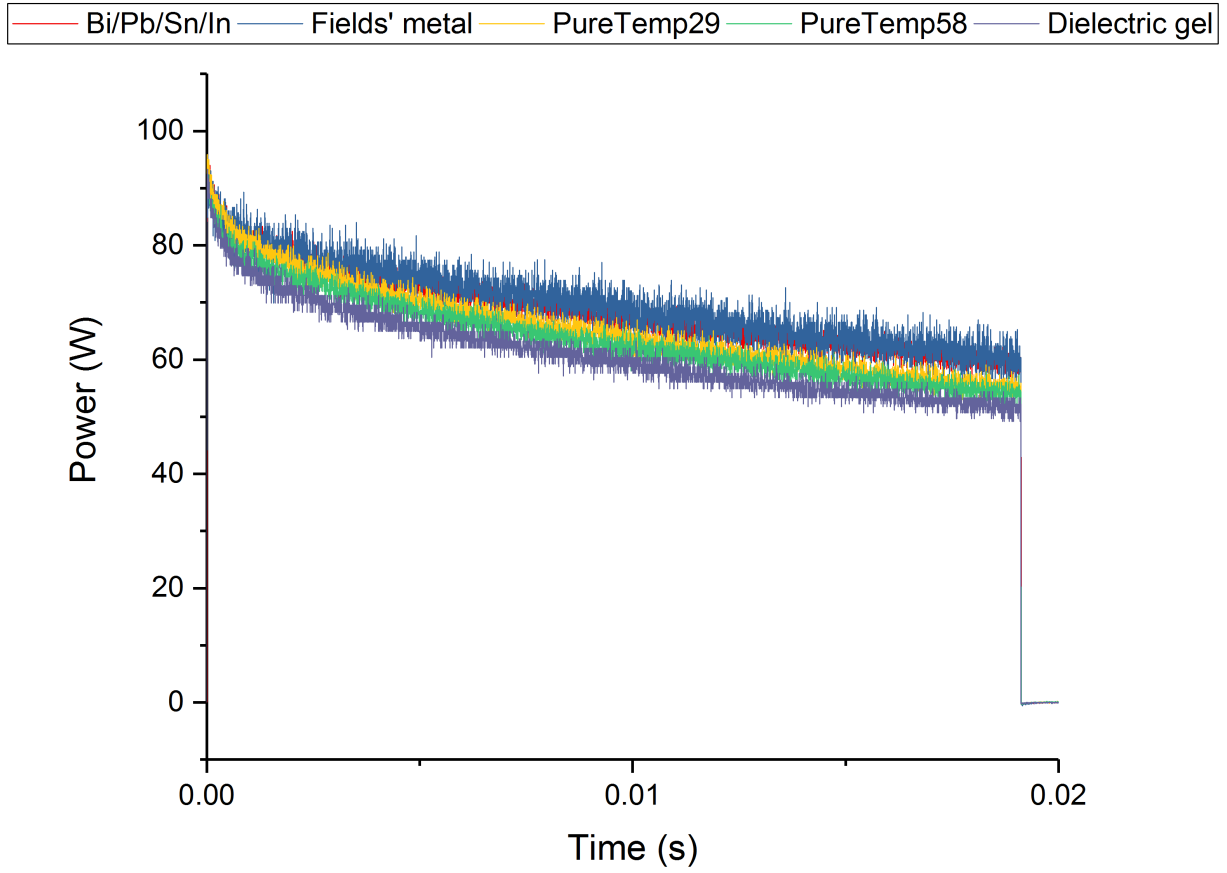
Power input plots for all devices under 40W pulse.



*An error occurred during the power input measurement for PureTemp58. Therefore, that is not the real power input in that case.

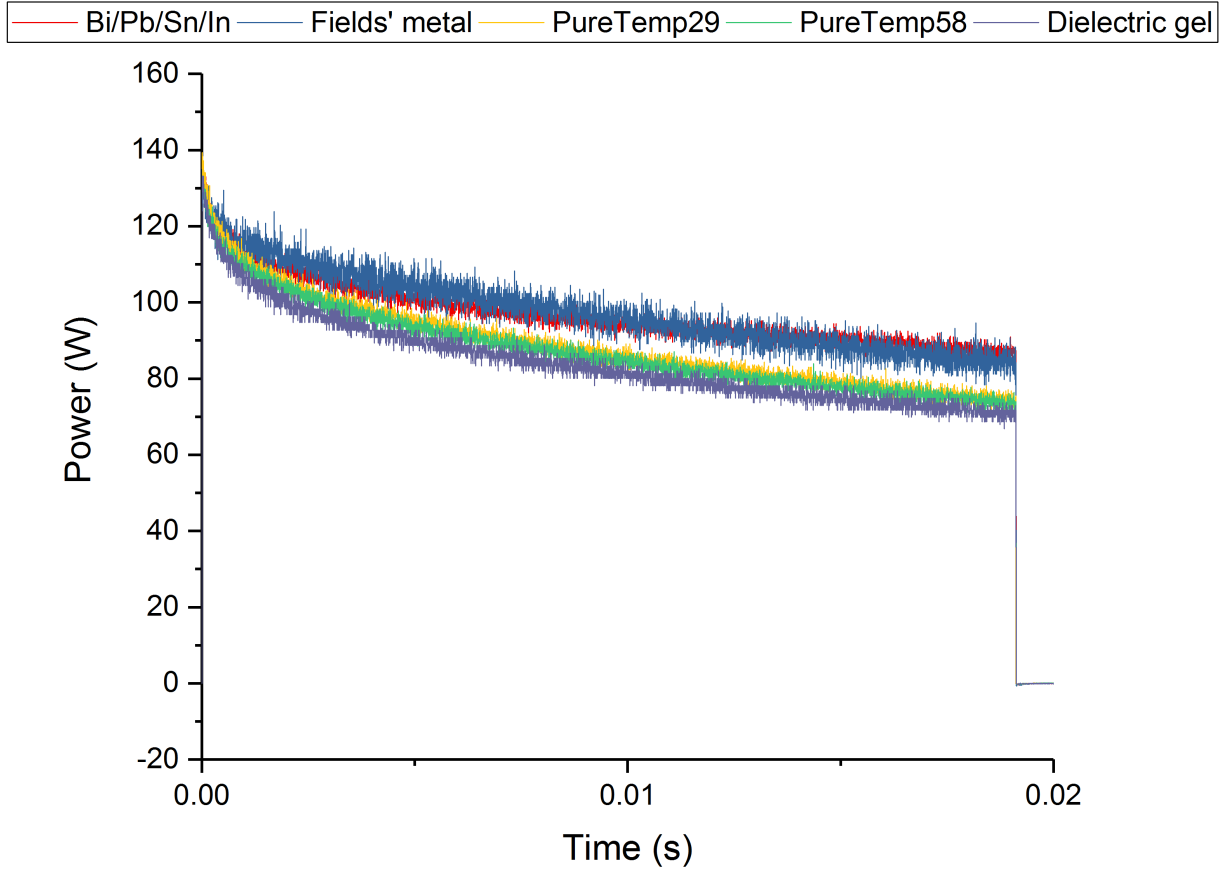
APPENDIX D

Power input plots for all devices under 80W pulse.



APPENDIX E

Power input plots for all devices under 120W pulse.



APPENDIX F

Power input plots for all devices under 160W pulse.

